

A Contemporary Survey on Fluid Antenna Systems: Fundamentals and Networking Perspectives

Hanjiang Hong, *Member, IEEE*, Kai-Kit Wong, *Fellow, IEEE*, Hao Xu, *Senior Member, IEEE*, Xinghao Guo, Farshad Rostami Ghadi, *Member, IEEE*, Yu Chen, *Member, IEEE*, Yin Xu, *Senior Member, IEEE*, Chan-Byoung Chae, *Fellow, IEEE*, Baiyang Liu, *Senior Member, IEEE*, Kin-Fai Tong, *Fellow, IEEE*, and Yangyang Zhang

Abstract—The explosive growth of teletraffic, fueled by the convergence of cyber-physical systems and data-intensive applications, such as the Internet of Things (IoT), autonomous systems, and immersive communications, demands a multidisciplinary suite of innovative solutions across the physical and network layers. Fluid antenna systems (FAS) represent a transformative advancement in antenna design, offering enhanced spatial degrees of freedom through dynamic reconfigurability. By exploiting spatial flexibility, FAS can adapt to varying channel conditions and optimize wireless performance, making it a highly promising candidate for next-generation communication networks. This paper provides a comprehensive survey of the state of the art in FAS research. We begin by examining key application scenarios in which FAS offers significant advantages. We then present the fundamental principles of FAS, covering channel measurement and modeling, single-user configurations, and the multi-user fluid antenna multiple access (FAMA) framework. Following this, we delve into key network-layer techniques such as quality-of-service (QoS) provisioning, power allocation, and content placement strategies. We conclude by identifying prevailing challenges and

outlining future research directions to support the continued development of FAS in next-generation wireless networks.

Index Terms—Fluid antenna system (FAS), channel modeling, homogeneous network (HomoNet), networking, physical layer.

I. INTRODUCTION

“Necessity is the mother of invention.”

FOR WIRELESS communications, this truism is the ultimate *raison d’être*. From the inception of wireless telegraphy in the late 19th century to the contemporary era when the next generation networks serve as indispensable conduits between the digital and physical realms, the unyielding demand for faster, smarter, and more reliable communications has been a continual catalyst for innovation. While fifth-generation (5G) networks have achieved significant advancements in data transmission speed, latency, and connectivity, these enhancements are insufficient to accommodate the evolving demands of the cyber-physical world. The forthcoming sixth-generation (6G) network is expected to overcome the constraints of its predecessor, aiming to meet highly ambitious key performance indicators (KPIs). These benchmarks include a peak data rate of 1 Tbps, an end-to-end latency of 1 ms, and an extraordinary connection density of 10 million devices per km², etc [1], [2], [3], [4]. Such objectives are not merely incremental upgrades. Rather, they are prerequisites for enabling the next generation of applications characterized by seamless interaction among humans, machines, and environments.

To achieve these goals, researchers are investigating a multidisciplinary suite of innovative solutions. These include non-orthogonal multiple access (NOMA) [5], [6], [7], rate-splitting multiple access (RSMA) [8], [9], extra-large multiple-output multiple-input (MIMO) [10], advanced coding and modulation schemes [11], [12], [13], and reconfigurable intelligent surfaces (RIS) [14], [15], [16]. Researchers are increasingly focusing on the development of advanced networks driven by artificial intelligence (AI) and learning-based methods [17], [18], [19], Terahertz (THz) communications [20], [21], [22], non-terrestrial networks (NTNs) [23], [24], and integrated sensing and communication (ISAC) [25], [26], [27], etc. NOMA and RSMA utilizes advanced coding and decoding architectures to allow more spectrum sharing for greater capacity while RIS extends the principle of MIMO to be used at programmable metasurfaces in remote areas for passive but smart reflections.

The work of K. K. Wong and F. Rostami Ghadi is supported by the Engineering and Physical Sciences Research Council (EPSRC) under Grant EP/W026813/1.

The work of H. Hong is supported by the Outstanding Doctoral Graduates Development Scholarship of Shanghai Jiao Tong University.

The work of H. Xu is supported by the Fundamental Research Funds for the Central Universities under grant 2242025R10001.

The work of Y. Xu and X. Guo is supported by National Natural Science Foundation of China Program (62371291,62422111).

The work of C.-B. Chae was in part supported by the Institute for Information and Communication Technology Planning and Evaluation (IITP)/NRF grant funded by the Ministry of Science and ICT (MSIT), South Korea, under Grant RS-2024-00428780 and 2022R1A5A1027646.

The work of K. F. Tong and B. Liu was funded by the Hong Kong Metropolitan University, Staff Research Startup Fund: FRSF/2024/03.

H. Hong, K. K. Wong, and F. Rostami Ghadi are with the Department of Electronic and Electrical Engineering, University College London, WC1E 7JE, London, United Kingdom. K. K. Wong is also affiliated with Yonsei Frontier Lab, Yonsei University, Seoul, South Korea (e-mail: {hanjiang.hong, kai-kit.wong, f.rostamighadi}@ucl.ac.uk).

H. Xu is with the National Mobile Communications Research Laboratory, Southeast University, Nanjing 210096, China (e-mail: hao.xu@seu.ac.cn).

X. Guo and Y. Xu are with the School of Information Science and Electronic Engineering, Shanghai Jiao Tong University, Shanghai 200240, China (e-mail: {guoxinghao, xuyin}@sjtu.edu.cn).

Y. Chen is with the School of Information and Communication Engineering, Beijing University of Posts and Telecommunications, Beijing 100876, China (e-mail: yu.chen@bupt.edu.cn).

C.-B. Chae is with the School of Integrated Technology, Yonsei University, Seoul, 03722 South Korea (e-mail: cbchae@yonsei.ac.kr).

B. Liu and K. F. Tong are with the School of Science and Technology, Hong Kong Metropolitan University, Hong Kong SAR, China (e-mail: {byliu, ktong}@hkmu.edu.hk).

Y. Zhang is with Kuang-Chi Science Limited, Hong Kong SAR, China (e-mail: yangyang.zhang@kuang-chi.org).

Corresponding author: Kai-Kit Wong.

Nevertheless, scalability remains a critical limitation of these technologies. On the other hand, while AI is a powerful tool for optimization and resource allocation of wireless networks, AI itself is not a wireless communication technology. Shifting to the THz band is clearly a natural approach to access greater bandwidth, although the associated high cost poses a major challenge. The deployment of NTN are application-specific. Evidently, ISAC makes communication more interesting but it also makes it a lot more difficult. In short, it remains essential to develop new technologies that introduce additional degree-of-freedom (DoF) at the physical layer, thereby expanding the achievable performance region, desperately needed for 6G.

To push the boundaries of physical-layer design, the fluid antenna system (FAS) stands out as a breakthrough technology, introducing dynamic reconfigurability in antenna position and structure, marking a leap in enhancing spatial DoF [28], [29]. Unlike conventional fixed-position antennas (FPA), a.k.a. traditional antenna system (TAS), a FAS is a software-defined architecture that uses fluidic, conductive, or dielectric materials to facilitate real-time reconfiguration of antenna position and shape in a given spatial region. This innate adaptability constitutes an integral part of the FAS design, introducing additional DoFs that can be exploited to achieve significant performance enhancements. FAS was first conceptualized by Wong *et al.* in 2020 [28], [30], [31], with its foundational idea partly inspired by Bruce Lee’s philosophy of adaptability and flow:

“Be like water making its way through cracks. Do not be assertive, but adjust to the object, and you shall find a way round or through it. If nothing within you stays rigid, outward things will disclose themselves. Empty your mind, be formless. Shapeless, like water. If you put water into a cup, it becomes the cup. You put water into a bottle and it becomes the bottle. You put it in a teapot it becomes the teapot. Now, water can flow or it can crash. Be water, my friend.”

Applying this philosophy to the physical layer of wireless communication leads to the conception of antennas that are inherently formless and highly adaptable, capable of dynamically reconfiguring themselves to cater to varying operational conditions. This idea is embodied in the FAS, which emphasizes extreme spatial reconfigurability and flexibility, marking a significant evolution in contemporary antenna design. The term ‘fluid’ in FAS highlights the system’s ability to rapidly adapt its configuration, without necessarily referring to liquid or gaseous states. Instead, it reflects the innovative, dynamic, and responsive nature of the architecture. FAS can be realized through various technological implementations, such as liquid-based antennas [32], [33], [34], pixel-reconfigurable antennas [35], [36], mechanically actuated antennas using stepper motors [37], and flexible structures incorporating metamaterials [38], [39], [40]. In essence, FAS encompasses all forms of flexible and reconfigurable antennas that adhere to its underlying principle of spatial adaptability, which includes movable antennas [41], pinching antennas [42], and the reconfigurable waveguide technology presented in [43] when all the intelli-

gent surfaces together combine to become an enormous FAS (E-FAS). Credit is also due to the foundational studies in [44], [45], [46], which first explored reconfigurable antennas in the context of space-time coding and beamforming.

The motivations for this survey are multifaceted. In recent years, FASs have attracted growing attention due to significant theoretical progress and their potential for a wide range of applications. Several review and tutorial articles have already explored various aspects of FAS. For example, [29] identified six key research areas and discussed the promise of FAS under simplified channel models. In [41], the historical development of FAS and movable antennas was comparatively analyzed, while [47] examined the interplay between FAS, MIMO, and RIS. Additional works, such as [48], [49], [50], have provided insights into the fundamental concepts of FAS, highlighted emerging research directions, and introduced a novel paradigm incorporating multiple RISs as distributed artificial scattering surfaces to facilitate massive connectivity. The study in [51] presented a comprehensive taxonomy of FAS applications in multiple access environments, termed fluid antenna multiple access (FAMA), and examined its potential integration with other cutting-edge technologies. More recently, [52] presented a comprehensive tutorial on the physical-layer foundations and enabling technologies of FAS. Lu *et al.* in [53] also offer an electromagnetic perspective to explain FAS.

Despite these valuable contributions, a significant gap remains in the literature concerning networking technologies specifically designed for FAS. This paper intends to address that gap by presenting a comprehensive survey of FAS, with a particular focus on its integration into future 6G networks and the networking techniques required to fully harness its potential. In doing so, this work aims to advance a holistic understanding of FAS and its transformative role in shaping next-generation wireless communication systems.

The remainder of this survey is organized as follows. Section II introduces the main scenarios and use applications of FAS in wireless communication networks. Section III then discusses the fundamentals of FAS, including the measurement and modeling of FAS channels, as well as the physical technologies of single-user FAS and multi-user FAMA systems. In Section IV, we investigate relevant network techniques, such as quality of service (QoS) enhancement, power allocation, and content placement. Section V identifies challenges and research directions, while Section VI concludes the paper.

II. APPLICATION SCENARIOS

This section explores various application scenarios for FAS, highlighting the core operational characteristics that define their relevance. These application scenarios serve as a foundation for developing key enabling techniques tailored to FAS. Traditionally, most FAS deployments have been limited to homogeneous networks (HomoNets), characterized by macro-cell-only infrastructure. As shown in Table I, these HomoNet scenarios can be broadly classified into two categories: Case 1, involving *single-user FAS networks*, and Case 2, involving *multi-user FAS networks*. More recently, FAS-assisted heterogeneous networks (HetNets) have gained attention, featuring

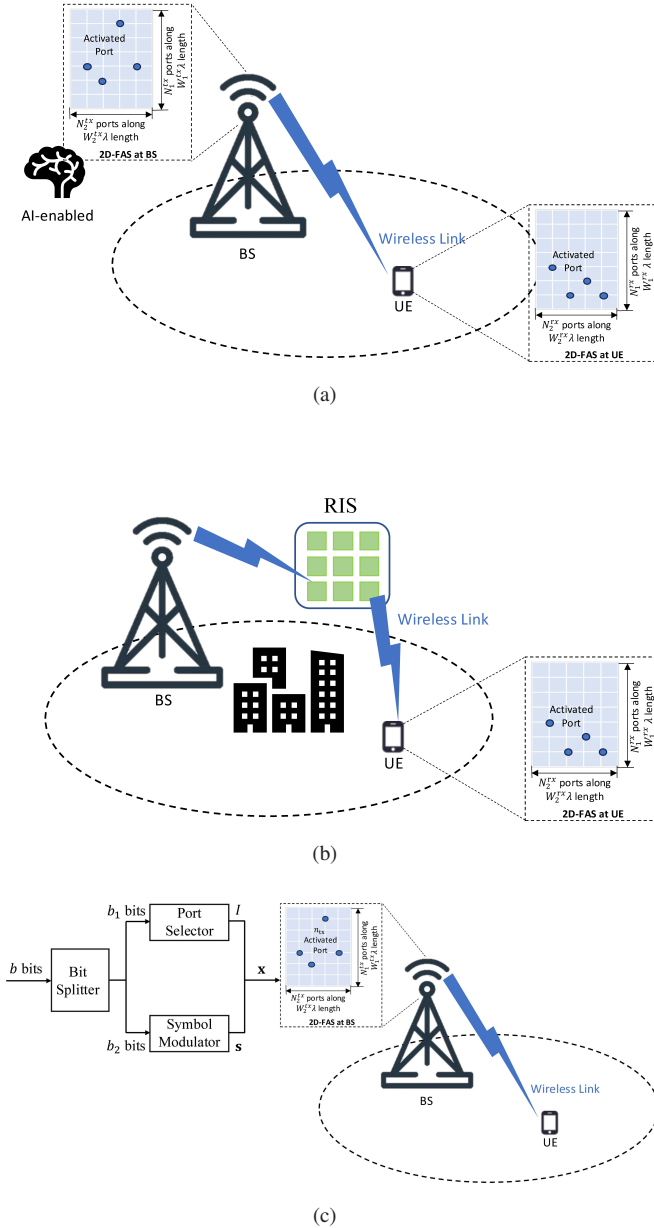


Fig. 1. Illustration of (a) Case 1A: Basic FAS, (b) Case 1B: RIS-aided FAS, and (c) Case 1C: FAS-aided IM.

integrated macro-cell and small-cell deployments. The following sections delve deeper into each of these scenarios.

A. Case 1: Single-user HomoNet FAS Scenarios

1) *Case 1A: Basic FAS*: In a basic FAS network, as shown in Fig. 1(a), FAS can be utilized at the transmitter and/or receiver. The basic FAS can be further categorized into two types based on the number of activated ports: single-input single-output FAS (SISO-FAS), which employs a single activated port, and MIMO-FAS, which utilizes multiple activated ports. For clarity, the subscript/superscript s is used to denote the parameters at the transmitter or receiver as tx or rx, respectively, i.e., $s \in \{\text{tx}, \text{rx}\}$. In this case, N_i^s ports are uniformly distributed along a linear segment of length $W_i^s \lambda$, in which $i \in \{1, 2\}$, $N_s = N_1^s \times N_2^s$ and $W_s = W_1^s \lambda \times W_2^s \lambda$. If $N_2^s = 1$,

the FAS configuration can be regarded as a one-dimensional linear FAS (1D-FAS); otherwise, if $N_i^s > 1$, $\forall i \in \{1, 2\}$, the configuration is considered as a two-dimensional planar FAS (2D-FAS). FAS is switched to the port(s) with the strongest signal to enhance the receiving performance.

Based on a simplified channel model, an early study in [29] shows that the outage probability of SISO-FAS decreases with the number of ports, and FAS could outperform maximal-ratio combining (MRC) when the number of ports is sufficiently large. The effort in [30] further derived the ergodic capacity and its lower bound, as well as the level crossing rate (LCR) and average fade duration (AFD). In [54], an efficient port selection method for the SISO-FAS network that combines machine learning methods with analytical approximations, was proposed using only a few port observations. In [55], the outage probability and diversity gain of SISO-FAS were derived using a simple yet accurate channel model that closely follows the spatial correlation of Jake's model, and an algorithm was proposed to approximate the value of the number of ports, N^* , at which the diversity gain saturates. Additionally, the performance of backscatter communication in SISO-FAS was analyzed in [56]. Moreover, secure communication for a SISO-FAS network was investigated in [57], where the key secrecy metrics, including secrecy outage probability, average secrecy capacity, and secrecy energy efficiency (EE) were analyzed.

Utilizing multiple fluid antennas at both ends of a point-to-point communication channel, referred to as MIMO-FAS, can provide enhanced performance compared with SISO-FAS and has recently been studied in [58]. Specifically, the diversity-and-multiplexing trade-off (DMT) for the MIMO-FAS channel was characterized at high signal-to-noise ratio (SNR). Besides, [59] addressed the MIMO-FAS channel exploiting only statistical channel state information (CSI). Based on the rate maximization criterion, an algorithmic framework was proposed for transmit precoding and transmit/receive FAS position designs. Later in [60], the problem of antenna configuration selection for MIMO-FAS was studied using physics-inspired heuristics to maximize two fundamental performance metrics: the SNR at the receiver side and the end-to-end Shannon capacity. In [61], the port selection problem on both the transmitter and receiver in MIMO-FAS was tackled to maximize the capacity. A new joint convex relaxation (JCR) problem is formulated, and two optimization algorithms are developed, each offering a different trade-off between performance and complexity.

2) *Case 1B: RIS-aided FAS*: RISs have emerged as a cost-effective technology for improving base station (BS) coverage by intelligently manipulating the propagation environment. By adjusting the phase shifts of their reflecting elements, RIS can steer radio signals toward intended receivers. When combined with FAS, RIS can produce synergistic performance gains. As shown in Fig. 1(b), the RIS-assisted FAS network comprises a BS equipped with a single FPA, a RIS with M reflecting elements, and a mobile user equipped with a FAS featuring N_{rx} ports. In this scenario, the direct link between the BS and the user is obstructed by physical obstacles. As a result, the BS transmits the RF signal, which is redirected by the RIS to reach the mobile receiver. The FAS-assisted mobile receiver demonstrates superb performance, effectively mitigating the double-

TABLE I
TYPICAL APPLICATION SCENARIOS

Type	Description	Features
Single-user HomoNet	Case 1A	Basic FAS ○ Enhanced performance and increasing capacity.
	Case 1B	RIS-aided FAS ○ Effectively mitigating the double-path loss of RIS.
	Case 1C	FAS-aided IM ○ Improving spectral efficiency.
Multi-user HomoNet	Case 2A	Multi-user MIMO-FAS ○ Improving robustness and capacity.
	Case 2B	FAMA ○ Massive connectivity.
	Case 2C	FAS-aided ISAC ○ Adaptive performance tuning; ○ Improving spectral efficiency.
HetNet	Case 3	Content-centric FAS HetNets ○ Enabling adaptive link establishment; ○ Improving spectral efficiency; ○ Enhancing reliability and robustness.

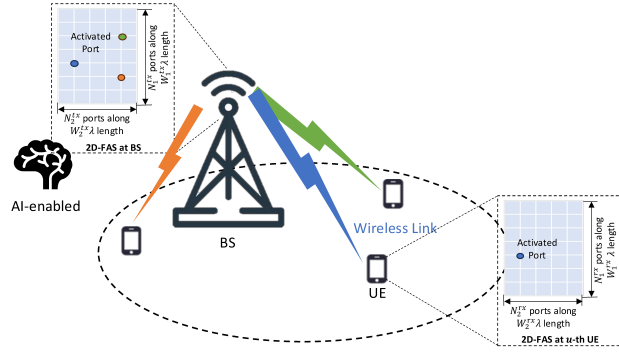
path loss in cascaded RIS systems [50], [62]. By applying the central limit theorem (CLT) and the block-correlation channel model, [63] simplified the expressions for outage probability, reduced computational complexity, and analyzed the impact of the number of FAS ports on system performance. In [64], the authors further derived the upper bound, lower bound, and asymptotic approximation of the outage probability. Additionally, the analytical outage probability expression was used to design the passive beamforming of the RIS. A framework for the RIS-aided FAS design was given in [65], proposing two approaches: a CSI-based scheme and a CSI-free scheme. Then leveraging the derived outage probabilities, [65] optimized the throughput of the RIS-aided FAS. It is also possible to come up with a low-complexity beamforming design for RIS-aided systems if a fluid antenna array exploiting only statistical CSI is used at the BS [66]. Subsequently, [67] studied the impact of RIS-FAS for secure communication, in which an analytical expression for the secrecy outage probability was obtained. In [68], a simultaneously transmitting and reflecting (STAR)-RIS system with FAS under phase errors, was investigated and the benefits of position reconfigurability was highlighted.

3) *Case 1C: FAS-aided IM*: Index modulation (IM) leverages the indices of entities to encode and transmit information. FAS can be utilized as the encoded entities in IM to enhance the overall performance. As illustrated in Fig. 1(c), the FAS-aided IM network consists of the transmitter equipped with FAS, and the receiver equipped with N_{rx} FPAs. The configuration of the FAS equipped at the transmitter is consistent with those in the aforementioned scenarios. The IM mechanism is applied to the fluid antenna ports, selecting n_{tx} ports out of N_{tx} ports for transmitting modulated symbols [69], [70], [71], [72]. Specifically, during each transmission interval, the input b -bit sequence is divided into two parts. The first part is mapped into n_{tx} Q_m -ary constellation symbols, represented as $\mathbf{s} = [s_1, \dots, s_k, \dots, s_{n_{\text{tx}}}]^T$, while the second part is mapped to an index set of n_{tx} ports, denoted as $\mathcal{I} = \{I_1, \dots, I_k, \dots, I_{n_{\text{tx}}}\}$, where $I_k \in \{1, 2, \dots, N_{\text{tx}}\}$. Therefore, the length of the first part is calculated as $b_1 = n_{\text{tx}} \log_2 M$, while that of the second part is calculated as $b_2 = \lfloor \log_2 \binom{N_{\text{tx}}}{n_{\text{tx}}} \rfloor$. The spectral efficiency of the FAS-aided IM network is therefore enhanced by the

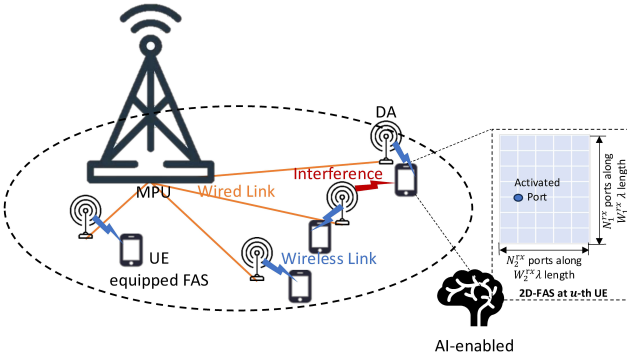
adequate possibility provided by the FAS port selection. In the initial studies, only one activated FAS port is considered for IM [69]. As the study progresses, FAS-aided IM with multiple activated ports is proposed [70]. To enhance spectral efficiency, [71] applies the FAS-aided IM to MIMO systems, and [72] further enhances the resilience of the systems in the spatial correlated channels. Also, [73] proposes a secure FAS-aided IM framework that safeguards both index and data symbol transmissions against eavesdropping by employing a combined configuration of non-orthogonal spectrally efficient frequency division multiplexing waveforms and channel coding. Then [74] combines FAS-aided IM with orthogonal frequency division multiplexing (OFDM) transmission systems and implements a wavelet scattering neural network in the proposed framework, achieving fast classification of index patterns using limited training data. A joint transmit and receive FAS-aided IM system enabled by RIS is also proposed in [75].

B. Case 2: Multi-user HomoNet FAS Scenarios

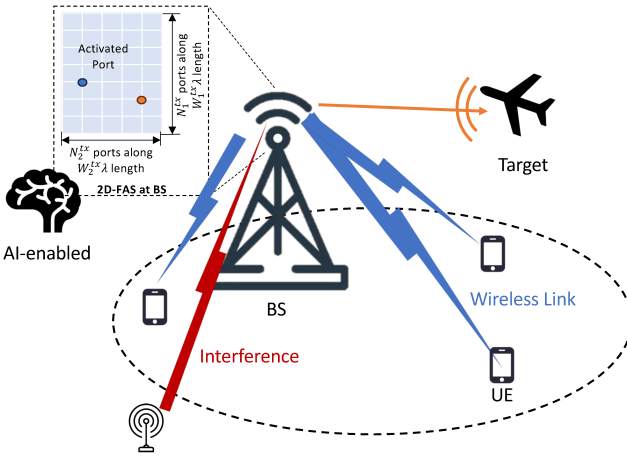
1) *Case 2A: Multi-user MIMO-FAS*: Multi-user MIMO-FAS (MU-MIMO-FAS) extends from the concept of MIMO-FAS and enhances the traditional MU-MIMO by leveraging FAS's spatial reconfigurability. As illustrated in Fig. 2(a), the BS serves U user equipments (UEs). Three scenarios can be considered: the first is to equip with a FAS with multiple RF chains at the BS and use a single traditional antenna with one RF chain on the UE side; the second is to use a multi-antenna uniform linear array (ULA) at the BS while each UE has a FAS; and the third is to adopt FAS on both sides. For the FAS at BS, $N_{\text{tx}} = N_1^{\text{tx}} \times N_2^{\text{tx}}$ antenna ports are uniformly distributed on a physical size of $W_{\text{tx}} = W_1^{\text{tx}} \lambda \times W_2^{\text{tx}} \lambda$. On the UE side, the distribution of the 2D-FAS can be denoted as $N_{\text{rx}} = N_1^{\text{rx}} \times N_2^{\text{rx}}$ ports over a size of $W_{\text{rx}} = W_1^{\text{rx}} \lambda \times W_2^{\text{rx}} \lambda$. FAS equipped on both sides can reduce the impact of hardware imperfections through dynamic antenna repositioning, thereby improving the robustness in MU-MIMO systems [76]. Moreover, FAS on the UE side enables sparse channel recovery via compressed sensing, achieving lower estimation errors compared to traditional fixed antennas [77], and it can greatly improve the capacity of multiple access channel in the uplink system [78].



(a)



(b)



(c)

Fig. 2. Illustration of (a) Case 2A: MU-MIMO-FAS, (b) Case 2B: FAMA, and (c) Case 2C: FAS-Aided ISAC.

2) *Case 2B: FAMA*: FAMA leverages the unique feature of FAS to capitalize on spatial opportunities where interference is weak. As illustrated in Fig. 2(b), the BS serves U UEs, each equipped with an $N_{rx} = N_1^{rx} \times N_2^{rx}$ ports FAS with a size of $W_{rx} = W_1^{rx} \lambda \times W_2^{rx} \lambda$. All U UEs reuse the same frequency radio resources. Thus, at each UE, interference channels with $(U - 1)$ UEs are considered. The UE uses FAS to identify and receive at the port with the weakest interference. Depending on how fast the UE updates the FAS port, FAMA can be roughly classified into *fast* FAMA (*f*-FAMA) [79], [80] or *slow* FAMA

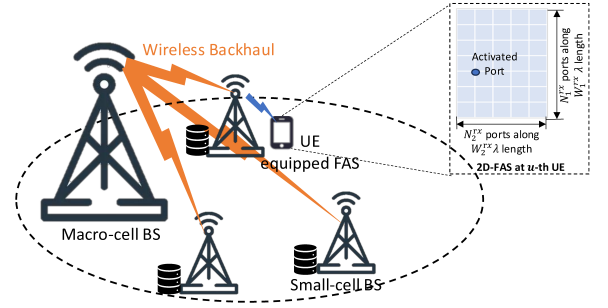


Fig. 3. Illustration of Case 3: FAS in a CCN.

(*s*-FAMA) [81]. The *f*-FAMA scheme switches the antenna port on a per-symbol basis, where the data-dependent sum interference plus noise signal cancels. This idea could achieve ultra-reliable massive access, supporting hundreds of users [80]. However, *f*-FAMA could be impractical because of the complexity of instantaneously observing a large number of received signals. On the contrary, *s*-FAMA is a more practical scheme because it only requires the FAS to switch the position once during each channel coherence time [82], [83]. Tens of users can be supported simultaneously by *s*-FAMA. As an evolution of *s*-FAMA, compact ultra massive antenna array (CUMA) [84] activates multiple antenna ports on the UE side to ensure that the received signals are combined constructively. Hence, the connectivity capability upgrades to hundreds of users again by CUMA [85]. Reinforcement learning is another promising solution to deal with the high-dynamic port selection [86]. Moreover, FAMA could be facilitated with coding and modulation to enhance its reliability [87], [88], [89].

3) *Case 2C: FAS-aided ISAC*: FAS enhance ISAC by dynamically balancing sensing and communication trade-offs. As illustrated in Fig. 2(c), the BS is equipped with a FAS and accommodates U users. The BS transmits common signals to the users and utilizes the echo signals to perform potential target sensing. For the FAS at BS, $N_{tx} = N_1^{tx} \times N_2^{tx}$ antenna ports are uniformly distributed on a physical size of $W_{tx} = W_1^{tx} \lambda \times W_2^{tx} \lambda$. FAS equipped at the BS can shift the ISAC Pareto frontier, enabling adaptive performance tuning [90]. In [91], reinforcement learning is used to optimize the antenna port selection and achieve 30% gains on spectral efficiency. FAS can also be equipped on the user side to improve backscatter device detection and spectral efficiency [92].

C. Case 3: Content-centric FAS HetNets

Recent advancements have further introduced FAS in Het-Net scenarios, particularly within the content-centric networks (CCNs) [93]. In CCNs, frequently accessed content is cached at small-cell BSs (SBSs) and/or edge nodes [94]. This mechanism effectively reduces end-to-end latency and alleviates backhaul load, which is essential for future 6G networks that demand ultra-low latency and high throughput with minimal infrastructural overhead. As shown in Fig. 3, content caching in CCN-enabled HetNets ensures that data is closer to end-users, minimizing redundant core network transmissions.

D. Conclusion of Application Scenarios

In this section, typical application scenarios are categorized into three types: homogeneous single-user, homogeneous multi-user, and heterogeneous networks with FAS.

The majority of the state-of-art FAS scenarios are based on HomoNet, which primarily employs macro-cell deployment. We further delineate the HomoNet FAS scenario into two categories: single-user and multi-user HomoNet scenarios. The single-user HomoNet includes basic FAS, RIS-aided FAS, and FAS-aided IM. Basic FAS is designed to enhance the performance and capacity of the network. In the RIS-aided FAS network, FAS effectively addresses the double-path loss of RIS. Furthermore, FAS-aided IM contributes to improving spectral efficiency. In the context of the multi-user HomoNet with FAS, three typical application scenarios emerge: MU-MIMO-FAS, FAMA, and FAS-aided ISAC. MU-MIMO-FAS is capable of enhancing both robustness and capacity; FAMA facilitates massive connectivity; and FAS-aided ISAC not only improves spectral efficiency but also offers adaptive performance tuning. In HetNet, FAS has recently been integrated into the content-centric HetNets, enabling adaptive link establishment, enhancing spectral efficiency, and improving the reliability and robustness of the networks.

Additionally, AI technologies play a critical role within various FAS network scenarios [95]. The key challenge addressed by deep learning approaches in FAS networks pertains to the port selection problem [54], [86], [96]. Deep learning methodologies can effectively tackle the high dynamics associated with channel adaptation in the port selection problem, yielding substantial improvements in spectral efficiency, connectivity, and flexibility within FAS-aided networks.

III. FUNDAMENTALS OF FAS

As FAS constitutes an emerging technology, channel modeling serves as a crucial aspect for assessing its performance. Moreover, the foundational techniques developed for FAS-aided systems predominantly concentrate on either single-user FAS or multi-user FAMA. This section presents an overview of the fundamentals of FAS, including its channel model, channel estimation, FAS, and FAMA.

A. Channel Model

We present channel models for both rich scattering and finite scattering environments, focusing on two FAS configurations: 1D-FAS and 2D-FAS. Without loss of generality, we assume a point-to-point channel where the transmitter utilizes a single FPA and the receiver employs a FAS.

1) *Rich-Scattering Environment*: For the 1D-FAS scenario, the receiver has a 1D-FAS with N ports, where the channel vector $\mathbf{h} = [h_1, \dots, h_N]^T$ captures the gains from the transmitter to FAS ports, with $h_n \sim \mathcal{CN}(0, \sigma^2)$. Due to the proximity of the ports, \mathbf{h} exhibits strong spatial correlation, characterized by the covariance matrix $\mathbf{J} = \sigma^2 \mathbf{\Sigma}$. Following the Jake's model [97], the (n, m) -th element of $\mathbf{\Sigma}$ is given by

$$(\mathbf{\Sigma})_{n,m} = \frac{1}{\sigma^2} \text{Cov}[h_n, h_m] = J_0\left(\frac{2\pi(n-m)}{N-1}W\right), \quad (1)$$

where $J_0(\cdot)$ denotes the zero-order Bessel function of the first kind. For performance analysis, the channel model \mathbf{h} must capture spatial correlation properties while remaining analytically tractable. Previous works [29] and [79] simplified the channel coefficients for the n -th port as

$$h_n = \sigma \left(\sqrt{1 - \mu_n^2} x_n + \mu_n x_0 \right) + j\sigma \left(\sqrt{1 - \mu_n^2} y_n + \mu_n y_0 \right), \quad \text{for } n = 1, \dots, N, \quad (2)$$

where $x_0, \dots, x_N, y_0, \dots, y_N$ follow independent and identically distributed (i.i.d.) $\mathcal{N}(0, \frac{1}{2})$, and μ_n is simplified as

$$\mu_n = J_0\left(\frac{2\pi(n-1)}{N-1}W\right). \quad (3)$$

While this model simplifies FAS performance analysis, it relies on the first port as a reference, potentially overlooking interdependencies among other ports, as noted in (1), which may lead to overly optimistic performance evaluations.

Several studies have enhanced the channel model (2). In particular, Wong *et al.* introduced an approach that replaces individual correlation parameters with a common parameter, μ , defined by [98]

$$\mu = \sqrt{2} \sqrt{{}_1F_2\left(\frac{1}{2}; 1, \frac{3}{2}; -\pi^2 W^2\right) - \frac{J_1(2\pi W)}{2\pi W}}, \quad (4)$$

where ${}_1F_2(\cdot; \cdot; \cdot)$ is the generalized hypergeometric function and $J_1(\cdot)$ is the first-order Bessel function of the first kind. This approach establishes mutual correlations among all ports within a FAS, allowing any port to serve as a reference. Building upon this model, [98] conducted a thorough analysis of both outage probability and multiplexing gain, while [99] explored optimal port selection strategies. However, the channel model provided by [98] still inadequately reflects the correlation among antenna ports as characterized by (1).

To improve accuracy, [100] introduced an innovative approach in which each channel coefficient is represented as a weighted linear combination of N i.i.d. complex Gaussian random variables. Specifically, let $\mathbf{U}\mathbf{A}\mathbf{U}^H$ denote the eigen-decomposition of $\mathbf{\Sigma}$. The channel can be expressed as

$$\mathbf{h} = \sigma \mathbf{U} \mathbf{A}^{\frac{1}{2}} \mathbf{g}, \quad (5)$$

where $\mathbf{g} = [g_1, \dots, g_N]^T \sim \mathcal{CN}(\mathbf{0}, \mathbf{I}_N)$. Accordingly, the n -th element of \mathbf{h} can be expressed as

$$h_n = \sigma \sum_{m=1}^N \sqrt{\lambda_m} u_{n,m} g_m = \sigma \sum_{m=1}^N \sqrt{\lambda_m} u_{n,m} (a_m + ib_m), \quad (6)$$

where $u_{n,m}$ is the (n, m) -th element of \mathbf{U} , and a_m and b_m are random variables distributed as $\mathcal{N}(0, \frac{1}{2})$. It is evident that \mathbf{h} designed in (5) or (6) adheres to the specified distribution, i.e., $\mathbf{h} \sim \mathcal{CN}(\mathbf{0}, \sigma^2 \mathbf{A})$. Nevertheless, while this ‘‘perfect’’ model offers theoretical precision, it is constrained by complex nested integrals as documented in [101]. To simplify, [100] and [101] proposed a simplification model. The covariance matrix $\mathbf{\Sigma}$ of \mathbf{h} exhibits a Hermitian Toeplitz structure, where the

eigenvalue concentration allows approximation using $M \ll N$ eigenvalues. Using the model, [100], [101] analyzed the outage probability for single- and two-user FASs, respectively.

For 2D-FAS, the receiver employs a 2D-FAS of size $W_1\lambda \times W_2\lambda$, which has a uniform grid structure with $N = N_1 \times N_2$ ports. Ports are indexed from left to right and bottom to top along, with index assignment given by

$$n = (n_2 - 1)N_1 + n_1. \quad (7)$$

The element $(\boldsymbol{\Sigma})_{n,m}$ describing the correlation between the ports $(n_1, n_2) \rightarrow n$ and $(m_1, m_2) \rightarrow m$ in the correlation matrix $\mathbf{J} = \sigma^2 \boldsymbol{\Sigma} \in \mathbb{C}^{N \times N}$ is given by

$$(\boldsymbol{\Sigma})_{n,m} = j_0 \left(2\pi \sqrt{\left(\frac{n_1 - m_1}{N_1 - 1} W_1 \right)^2 + \left(\frac{n_2 - m_2}{N_2 - 1} W_2 \right)^2} \right), \quad (8)$$

where $j_0(\cdot)$ is the spherical Bessel function of the first kind. Similarly, with the eigen-decomposition $\boldsymbol{\Sigma} = \mathbf{U} \boldsymbol{\Lambda} \mathbf{U}^H$, the complex channel vector can be modeled as in (5) or (6) [55].

In [58], the channel model is extended to the case where both the transmitter and the receiver use a FAS, and multiple ports can be activated. In this case, SISO-FAS is extended to MIMO-FAS, and the complex channel becomes

$$\mathbf{H} = \mathbf{U}_{\text{rx}} \sqrt{\boldsymbol{\Lambda}_{\text{rx}}} \mathbf{G} \sqrt{\boldsymbol{\Lambda}_{\text{tx}}} \mathbf{U}_{\text{tx}}^H, \quad (9)$$

where $\mathbf{G} \in \mathbb{C}^{N_{\text{rx}} \times N_{\text{tx}}}$ with each entry being i.i.d. and following the distribution $\mathcal{CN}(0, 1)$, \mathbf{U}_s is an $N_s \times N_s$ matrix whose columns are the eigenvectors of \mathbf{J}_s and $\boldsymbol{\Lambda}_s = \text{diag}(\lambda_1^s, \dots, \lambda_{N_s}^s)$ is an $N_s \times N_s$ diagonal matrix whose diagonal entries are the corresponding eigenvalues, $s \in \{\text{tx}, \text{rx}\}$.

2) *Finite-Scattering Environment*: In a finite-scattering environment such as millimeter-wave communication systems, the planar-wave geometric model effectively characterizes the channel [102]. In this case, \mathbf{h} is modeled as

$$\mathbf{h} = \sqrt{N} \sum_{l=1}^L \gamma_l \mathbf{a}_l, \quad (10)$$

where L is the number of propagation paths and γ_l is the complex channel gain of the l -th path, \mathbf{a}_l is the steering vector at the receiver. This steering vector for 1D-FAS is given by

$$\mathbf{a}_l = \frac{1}{\sqrt{N}} \left[1, e^{-j \frac{2\pi}{\lambda} \Delta \cos \phi_l}, \dots, e^{-j \frac{2\pi}{\lambda} (N-1) \Delta \cos \phi_l} \right]^T, \quad (11)$$

where $\phi_l \in [0, \pi]$ is the angle-of-arrival (AoA) of the l -th propagation path and $\Delta = W\lambda/(N-1)$ is the distance between any two adjacent ports.

In 2D-FAS, the FAS surface lies on the x-y plane. The vector of the (n_1, n_2) -th port within the three-dimensional (3D) coordinate is therefore $[(n_1 - 1)\Delta_1, (n_2 - 1)\Delta_2, 0]$, where $\Delta_1 = W_1\lambda/(N_1 - 1)$ and $\Delta_2 = W_2\lambda/(N_2 - 1)$. Let the elevation and azimuth AoAs for the l -th propagation path be denoted by $\theta_l \in [0, \pi]$ and $\phi_l \in [0, \pi]$, respectively. The propagation difference of the l -th path between ports (1, 1) and (n_1, n_2) is then given by

$$s_l(n_1, n_2) = (n_1 - 1)\Delta_1 \sin \theta_l \cos \phi_l + (n_2 - 1)\Delta_2 \cos \theta_l, \quad (12)$$

resulting in phase difference $\frac{2\pi}{\lambda} s_l(n_1, n_2)$. The steering vector for 2D-FAS is defined as

$$\mathbf{a}_l = \frac{1}{\sqrt{N}} \left[1, e^{-j \frac{2\pi}{\lambda} s_l(1,2)}, \dots, e^{-j \frac{2\pi}{\lambda} s_l(N_1, N_2)} \right]^T. \quad (13)$$

B. Channel Estimation

To achieve best performance, reliable CSI for all ports is essential. Nevertheless, estimating CSI for all ports can lead to substantial hardware switching and system overhead. This subsection outlines the channel estimation process for FAS in rich-scattering and finite-scattering environments.

1) *Rich-Scattering Environment*: Several papers have investigated channel estimation in the rich-scattering environment. For instance, [103] and [104] investigated channel estimation and outage performance of large-scale cellular networks using circular multi-fluid antenna arrays. They proposed the skipped-enabled linear minimum mean square error (LMMSE)-based channel estimation (SeCE) technique, which reduces signaling overhead by estimating CSI for a select subset of ports, though it results in lower observed SINR and involves a trade-off between overhead reduction and SINR degradation.

Recent studies have highlighted the role of machine learning techniques in channel estimation for FAS. For instance, [105] showed how machine learning could recover full CSI from a limited number of ports, introducing specialized sub-networks for different conditions. In addition, they proposed a hard selection method to adjust the number of estimated ports based on correlation levels. In [106], the authors investigated spatial extrapolation using an asymmetric graph masked autoencoder (AGMAE) framework to address the complexities of high-resolution FAS, combining graph-based processing with an architecture that enhances generalization capability.

2) *Finite-Scattering Environment*: The channel estimation problem in finite-scattering environments has been studied in several works [77], [107], [108], [109], [110]. Here we focus on a typical multi-user uplink system described in [77]. In this context, each user employs a 1D-FAS, while the BS has M FPAs. Let $\mathbf{h}_{u,n} \in \mathbb{C}^{M \times 1}$ denote the channel vector from the n -th port of user u to the BS. By stacking $\mathbf{h}_{u,n}$ for all $n \in \{1, \dots, N\}$, we obtain the channel matrix between all ports of user u and the BS as

$$\mathbf{H}_u = [\mathbf{h}_{u,1}, \dots, \mathbf{h}_{u,N}]. \quad (14)$$

We introduce various schemes to estimate \mathbf{H}_u below.

a) *Least Square (LS) Scheme*: A basic approach to estimate \mathbf{H}_u involves all users sequentially transmitting orthogonal pilot sequences across N ports, each repeated T times. The LS estimate of $\mathbf{h}_{u,n}$ can be obtained by right-multiplying the normalized signal matrix with the corresponding pilot sequence, given by

$$\hat{\mathbf{h}}_{u,n}^{\text{LS}} = \mathbf{h}_{u,n} + \hat{\mathbf{z}}_{u,n}, \quad (15)$$

where $\hat{\mathbf{z}}_{u,n}$ is the estimation error caused by the additive noise. By stacking (15) for all n , the LS estimate of \mathbf{H}_u is

$$\hat{\mathbf{H}}_{u,\text{LS}} = \mathbf{H}_u + \hat{\mathbf{Z}}_u. \quad (16)$$

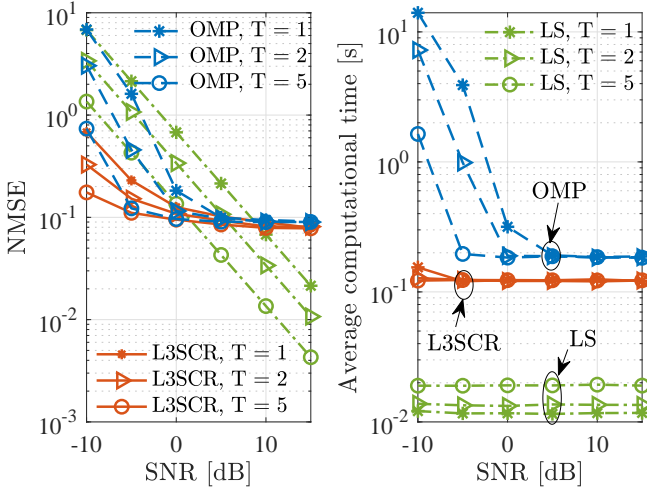


Fig. 4. NMSE and computational time with $M = 64$ and $K = 10$.

The accuracy of LS largely depends on the number of times a pilot sequence is repeated, i.e., T , and the transmit power. However, given that the number of ports N is typically large, LS method suffers from high hardware complexity and pilot overhead, making it impractical for real-world applications.

b) Low-Sample-Size Sparse Channel Reconstruction (L3SCR) Method: In a finite-scattering environment, the channel exhibits sparsity. In sparse channel environments, effective estimation can occur by limiting measurement to $K \ll N$ preset estimating locations (ELs). The channel vector from the k -th EL of user u is $\mathbf{g}_{u,k} \in \mathbb{C}^{M \times 1}$, and denote $\mathbf{G}_u = [\mathbf{g}_{u,1}, \dots, \mathbf{g}_{u,K}] \in \mathbb{C}^{M \times K}$. Using the planar-wave geometric channel model, \mathbf{G}_u can be expressed as

$$\mathbf{G}_u = \sqrt{MK} \sum_{l=1}^{L_u} \gamma_{u,l} \mathbf{a}_{u,R}(\phi_{u,l}) \mathbf{a}_{u,T}^H(\theta_{u,l}), \quad (17)$$

where L_u is the number of propagation paths between user u and the BS, $\gamma_{u,l}$ is the complex channel gain of the l -th path, and $\phi_{u,l}, \theta_{u,l} \in [0, \pi]$ are the corresponding AoA and AoD. In addition, $\mathbf{a}_{u,R}(\phi_{u,l})$ and $\mathbf{a}_{u,T}(\theta_{u,l})$ are respectively the steering vectors at the receiver and transmitter sides. In [77], a method called L3SCR is proposed to estimate the sparse channel parameters from \mathbf{G}_u and reconstruct \mathbf{H}_u .

c) Orthogonal Matching Pursuit (OMP) Algorithm: The accuracy of the L3SCR method depends significantly on the number of BS antennas, M . When M is sufficiently large, the estimates of the number of paths and AoAs are accurate. Otherwise, the accuracy of these estimates may be compromised. To mitigate this issue, the OMP algorithm can be utilized to enhance estimation accuracy, albeit at the expense of increased computational complexity. OMP jointly estimates the AoD and AoA in an iterative manner. Iteratively carry out the third to the fifth steps until the difference between consecutive residual vectors falls below a predefined threshold. Once the sparse parameters have been accurately estimated, the final step is to reconstruct the complete channel matrix using the approach employed in the L3SCR scheme.

Fig. 4 illustrate the normalized mean square error (NMSE) and the average computational time for one channel realization,

comparing different schemes across various parameters. In many scenarios, the LS method achieves a lower NMSE compared to both the L3SCR and OMP schemes. However, it is crucial to note that the LS method incurs significantly higher hardware switching and pilot overhead, as it requires the antennas of all users to switch and transmit pilot sequences across all N ports. This increased overhead can lead to a reduction in spectral efficiency. Additionally, it is evident that the OMP algorithm requires much more computational time than the L3SCR scheme. This is due to the fact that the OMP algorithm involves matrix inversions when solving LS problems, which is computationally intensive.

d) Other Schemes: In the previous two paragraphs, we show that in the finite-scattering environment, the geometric model can be adopted to characterize the channel of an FAS-assisted uplink system. In this case, standard tools can be used to estimate the sparse parameters at some preset ELs, based on which the CSI at all N ports can be reconstructed. In addition to the L3SCR and OMP methods, several other schemes can also be utilized for channel estimation in FAS-assisted systems. These include methods such as the multiple signal classification (MUSIC) technique [111], the estimation of signal parameters via rotational invariance technique (ESPRIT) [112], the unitary ESPRIT algorithm [113], and the space-alternating generalized expectation-maximization (SAGE) scheme [114], among others. These methods primarily differ in terms of the accuracy they provide in estimation and the computational complexity required for their implementation.

C. Single-user FAS and its Variants

1) Transmission Model: For a point-to-point FAS where the transmitter uses a fixed antenna, but the receiver has a fluid antenna with one activated port (i.e., SISO-FAS), the received signal at the n -th port of fluid antenna is given by

$$r_n = h_n s + \eta_n, \quad (18)$$

where h_n represents the complex channel coefficient at the n -th port, s is the transmitted information-bearing symbol and $\eta_n \sim \mathcal{CN}(0, \sigma_\eta^2)$ is the additive white Gaussian noise (AWGN). To achieve optimal performance, FAS activates the port corresponding to the strongest channel, i.e.,

$$h_{\text{FAS}} = \max_n \{|h_n|\}. \quad (19)$$

After selecting the optimal port, the rate of the SISO-FAS can be expressed as

$$R = \log \left(1 + \frac{\sigma_s^2}{\sigma_\eta^2} |h_{\text{FAS}}|^2 \right), \quad (20)$$

in which $\sigma_s^2 = \mathbb{E}\{|s|^2\}$. The outage probability of the SISO-FAS can be given by

$$p_{\text{SISO-FAS}} = \text{Prob} \left(\frac{\sigma_s^2}{\sigma_\eta^2} |h_{\text{FAS}}|^2 < \gamma \right), \quad (21)$$

where γ represents the SNR threshold. The outage probability of the SISO-FAS is derived in [55]. At high SNR the outage probability of SISO-FAS is given by [55, Theorem 2]

$$p_{\text{SISO-FAS}} = \frac{1}{\det(\mathbf{J})} \left(\frac{\gamma}{\Gamma} \right)^N + o(\Gamma^{-N}), \quad (22)$$

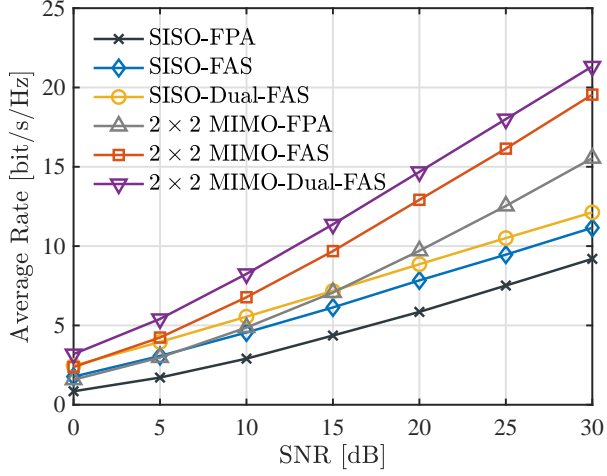


Fig. 5. Channel capacity of SISO-FAS and MIMO-FAS against SNR for FAS with $W_1^s = W_2^s = 0.5\lambda$ and $N_1^s = N_2^s = 4$ ($s \in \{\text{tx}, \text{rx}\}$).

where $\Gamma = \sigma_s^2/\sigma_\eta^2$ is the transmit SNR.

As illustrated in Fig. 1(a), fluid antenna can be adopted at both transmitter and receiver sides, and multiple ports can be activated. In this MIMO-FAS case, the channel of MIMO-FAS is given by (9). The activation port matrix is denoted as $\mathbf{A}_s = [\mathbf{a}_1^s, \dots, \mathbf{a}_{n_s}^s]$, where \mathbf{a}_l^s is the N_s -dimensional standard basis vector for $l \in \{1, 2, \dots, n_s\}$. The beamforming matrix is denoted as \mathbf{W}_s with the constraint $\|\mathbf{W}_s\|_2 = 1$. Then, the received signal of MIMO-FAS can be written as

$$\begin{aligned} \tilde{\mathbf{Y}} &= \mathbf{W}_{\text{rx}} \mathbf{A}_{\text{rx}} \mathbf{Y} \\ &= \mathbf{W}_{\text{rx}} \mathbf{A}_{\text{rx}} \mathbf{H} \mathbf{A}_{\text{tx}} \mathbf{W}_{\text{tx}} \mathbf{s} + \mathbf{W}_{\text{rx}} \mathbf{A}_{\text{rx}} \boldsymbol{\eta} \\ &\triangleq \tilde{\mathbf{H}} \mathbf{x} + \tilde{\boldsymbol{\eta}}, \end{aligned} \quad (23)$$

where \mathbf{s} is the transmitted signal and $\boldsymbol{\eta}$ is the AWGN. Denote $\tilde{\mathbf{H}} = \mathbf{A}_{\text{rx}} \mathbf{H} \mathbf{A}_{\text{tx}}$ and $\mathbf{K} = \mathbf{W}_{\text{tx}} \mathbf{P} \mathbf{W}_{\text{tx}}^H$, where \mathbf{K} is the input covariance and $\mathbf{P} = \mathbb{E}[\mathbf{s}\mathbf{s}^H]$ is the power allocation matrix. Then, the rate of MIMO-FAS can be expressed as

$$R = \log \det \left(\mathbf{I} + \tilde{\mathbf{H}} \mathbf{K} \tilde{\mathbf{H}}^H \right), \quad (24)$$

where the value of trace(\mathbf{K}) does not exceed the transmit SNR. The rate of MIMO-FAS can be maximized through joint optimization of port selection, transmit and receive beamforming, and power allocation. The solution can be obtained using an exhaustive search, singular value decomposition (SVD), and waterfilling for port selection, beamforming and power allocation, respectively, at the cost of high complexity. In [58], the joint optimization of the port activated matrices and beamforming matrices was addressed.

2) *Theoretical Performance*: Fig. 5 shows the rate of FAS compared to traditional FPA systems, where the ‘‘FAS’’ curves represent systems that employ a single fluid antenna at either the transmitter or receiver, and the ‘‘Dual-FAS’’ curves represent systems where fluid antennas are employed at both the transmitter and receiver. Therefore, the SISO-Dual-FAS curve can be viewed as a special case of MIMO-FAS when $n_s = 1$. Also, the fluid antennas all have the same specifications, i.e., $W_1^s = W_2^s = 0.5\lambda$ and $N_1^s = N_2^s = 4$, $s \in \{\text{tx}, \text{rx}\}$. It can be

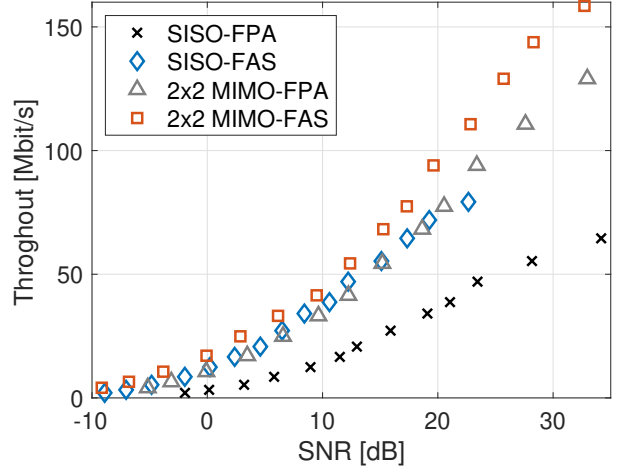


Fig. 6. Throughput against SNR in link-level simulations of 20 MHz bandwidth for FAS with $W_1^{\text{tx}} = W_2^{\text{tx}} = 0.5\lambda$ and $N_1^{\text{tx}} = N_2^{\text{tx}} = 4$.

observed that with the assistance of FAS, the channel capacity can be significantly improved, and when fluid antennas are simultaneously employed at the transmitter and receiver, the channel capacity can be further enhanced.

3) *Link-level Simulation Results*: Recently, [115] studied the use of FAS into the wideband 5G New Radio (NR) OFDM system and showed that FAS achieves significant gain in wideband systems. Results in Fig. 6 show the throughput of FAS with comparison to traditional FPA systems for different modulation and coding schemes. FAS is equipped at the receiver. The simulation bandwidth is set to be 20 MHz, with the delay spread $DS = 30$ ns and Doppler frequency $f_D = 30$ Hz. For FAS configuration, $N = 4 \times 4$ ports are distributed among FAS plane with the size of $W = 0.5\lambda \times 0.5\lambda$. It can be observed that FAS can improve the throughput in wideband channels. Specifically, SISO-FAS nearly double the throughput compared with FPA, and MIMO-FAS can further improve the throughput with a bit higher SNR.

4) *Variants of FAS*: The performance of FAS can be further enhanced with RIS. As seen in Fig. 1(b), in RIS-aided FAS, the received signal at the n -th port of the UE is written as

$$y_n = \sigma_s \sum_{m=1}^M h_m g_{m,n} e^{-j\theta_m} s + \eta_n, \quad (25)$$

where $h_m \sim \mathcal{CN}(0, \sigma_h^2)$ denotes the channel coefficient from the BS to the m -th RIS element, $g_{m,n} \sim \mathcal{CN}(0, \sigma_g^2)$ denotes the channel from the m -th RIS element to the n -th FAS port of the UE, θ_m denotes the reflecting phase of the m -th RIS element, $m = 1, \dots, M$, M is the number of RIS elements. By adjusting θ_m such that $\theta_m = -\arg(h_m g_{m,n})$, the channel gain can be maximized. As such, the UE will select and activate the port with the maximum combined channel gain, i.e.,

$$n^* = \arg \max_k \sum_{m=1}^M |h_m| |g_{m,n}|. \quad (26)$$

When FAS is implemented only at the transmitter, combining with IM can effectively enhance spectral efficiency. As il-

illustrated in Fig. 1(c), the transmitted signal vector $\mathbf{x} \in \mathbb{C}^{N_{tx} \times 1}$ in [71] can be represented as

$$\mathbf{x} = \sum_{i=1}^{n_{tx}} s_i \mathbf{e}_{I_i}, \quad (27)$$

where $s_i \in \mathcal{X}$, \mathcal{X} is a Q_m -ary modulation constellation, and \mathbf{e}_{I_i} denotes the N_{tx} -dimensional standard basis vector. The received signal vector $\mathbf{y} \in \mathbb{C}^{N_r \times 1}$ is given by

$$\mathbf{y} = \mathbf{H}\mathbf{x} + \boldsymbol{\eta}, \quad (28)$$

where \mathbf{H} represents the complex channel, which is given by (9), and $\boldsymbol{\eta}$ is the AWGN. Assuming the receiver has perfect knowledge of the CSI, the optimal maximum likelihood (ML) detector can be expressed as

$$\begin{aligned} (\hat{\mathcal{I}}, \hat{\mathbf{s}}) &= \arg \min_{\mathcal{I}, \mathbf{s}} \|\mathbf{y} - \mathbf{H}\mathbf{x}\|^2 \\ &= \arg \min_{\mathcal{I}, \mathbf{s}} \left\| \mathbf{y} - \mathbf{H} \sum_{k=1}^{n_{tx}} s_k \mathbf{e}_{I_k} \right\|^2. \end{aligned} \quad (29)$$

The spectral efficiency in terms of bits per channel use (bpcu), is formulated as

$$\text{SE} = n_{tx} \log_2 Q_m + \left\lfloor \log_2 \binom{N_{tx}}{n_{tx}} \right\rfloor \quad [\text{bpcu}]. \quad (30)$$

The $\left\lfloor \log_2 \binom{N_{tx}}{n_{tx}} \right\rfloor$ part of (30) is the additional spectral efficiency gained from IM.

D. Multi-user FAMA and its Variants

1) *Transmission Model*: As shown in Fig. 2(b), the received signal of at the n -th port of user u is modelled as

$$r_n^{(u)} = h_n^{(u,u)} s^{(u)} + \sum_{\substack{\tilde{u}=1 \\ \tilde{u} \neq u}}^U h_n^{(\tilde{u},u)} s^{(\tilde{u})} + \eta_n^{(u)}, \quad (31)$$

where $h_n^{(\tilde{u},u)}$ is the channel from the \tilde{u} -th BS antenna to UE u at the n -th port, $\eta_n^{(u)}$ is the AWGN with variance of σ_η^2 , and $s^{(u)}$ is the transmitted symbol for UE u with $\mathbb{E}[|s^{(u)}|^2] = \sigma_s^2$.

The key point of FAMA is to select the antenna port(s) with the highest SINR at each UE for multiple access, i.e.,

$$n^* = \arg \max_n \gamma_n, \quad n = 0, \dots, N^* - 1, \quad (32)$$

where γ_n is the SINR metric of the n -th port, whose definition varies between s -FAMA and f -FAMA.

In s -FAMA [81], γ_n is the average SINR calculated as

$$\gamma_n^{s\text{-FAMA}} = \frac{\sigma_s^2 |h_n^{(u,u)}|^2}{\sigma_s^2 \sum_{\substack{\tilde{u}=1 \\ \tilde{u} \neq u}}^U |h_n^{(\tilde{u},u)}|^2 + \sigma_\eta^2}. \quad (33)$$

The outage probability of s -FAMA is thus defined as

$$p_{s\text{-FAMA}} \triangleq \text{Prob} \left(\max_n \frac{\sigma_s^2 |h_n^{(u,u)}|^2}{\sigma_s^2 \sum_{\substack{\tilde{u}=1 \\ \tilde{u} \neq u}}^U |h_n^{(\tilde{u},u)}|^2 + \sigma_\eta^2} < \gamma \right), \quad (34)$$

where γ now denotes the SINR threshold.

For f -FAMA [79], [80], on the other hand, γ_n is the instantaneous SINR calculated as

$$\gamma_n^{f\text{-FAMA}} = \frac{|h_n^{(u,u)} s^{(u)}|^2}{|\tilde{h}_n^{(u)}|^2}, \quad (35)$$

where $\tilde{h}_n^{(u)} \triangleq \sum_{\substack{\tilde{u}=1 \\ \tilde{u} \neq u}}^U h_n^{(\tilde{u},u)} s^{(\tilde{u})} + \eta_n^{(u)}$ represents the instantaneous data-dependent interference and noise. The outage probability of s -FAMA can be defined as

$$p_{f\text{-FAMA}} \triangleq \text{Prob} \left(\max_n \frac{|h_n^{(u,u)} s^{(u)}|^2}{|\tilde{h}_n^{(u)}|^2} < \gamma \right). \quad (36)$$

The multiplexing gain that measures the capacity scaling is an important performance indicator in FAMA. Assume a fixed rate is transmitted to every user, the multiplexing gain in FAMA can be defined as

$$m_{\text{FAMA}} = (1 - p_{\text{FAMA}})U, \quad (37)$$

where p_{FAMA} is given by (34) or (36).

In the simplified channel model (2), if $|\mu_2| = \dots = |\mu_N| = \mu$, the outage probability of s -FAMA is upper bounded by [81, Theorem 3]

$$p_{s\text{-FAMA}} < \left[1 - N \left(\frac{\mu^2}{\gamma + 1} \right)^{U-1} - N \left(\frac{1 - \mu^2}{\gamma} \right)^{U-1} \right]^+, \quad (38)$$

where the operation $(a)^+ = \max\{0, a\}$ is to ensure that the bound is never negative. Hence, the multiplexing gain of the s -FAMA network, m , is bounded by [81, Theorem 4]

$$U \geq m \geq \min \left\{ NU \left(\frac{1 - \frac{1}{\pi W}}{\gamma} \right)^{U-1}, U \right\}. \quad (39)$$

In f -FAMA, the outage probability is upper bounded by [79, Theorem 3]

$$\begin{aligned} p_{f\text{-FAMA}} &\lesssim \frac{1 - \mu^2}{4\mu^2} \exp \frac{1 - \mu^2}{4\mu^2} \\ &\times \sum_{n=0}^{N-1} \frac{\binom{N-1}{n} (-1)^n}{\left(\frac{\sigma_s^2 \sigma_s^2 \gamma}{\sigma_\eta^2} \right)^n} e^{-\frac{n}{4}} E_k \left(\frac{n}{4} + \frac{1 - \mu^2}{4\mu^2} \right), \end{aligned} \quad (40)$$

where $E_k(\cdot)$ represents the generalized exponential integral, $\sigma_I^2 = \sum_{\substack{\tilde{u}=1 \\ \tilde{u} \neq u}}^U \mathbb{E}[|h_n^{(\tilde{u},u)}|^2] \sigma_s^2$ is the variance of interference.

Accordingly, the multiplexing gain of the f -FAMA network is bounded by [79, Corollary 2]

$$\begin{aligned} U \geq m &\gtrsim \min \left\{ \frac{(N-1)(1-\mu^2)U}{\left(\frac{\sigma_s^2 \sigma_s^2 \gamma}{\sigma_\eta^2} \right)}, U \right\} \\ &\approx \min \left\{ \frac{(N-1)(1-\mu^2)}{\gamma}, U \right\}. \end{aligned} \quad (41)$$

However, the channel model (2) is not quite accurate and may lead to artificially optimistic performance predictions as analyzed in Section III-A. Nevertheless, the derivation in the more accurate channel model (6) is much more complicated. The outage probability of the two-user FAMA case in the more accurate channel model (6) was derived in [83], and [82] derived the outage probability of s -FAMA.

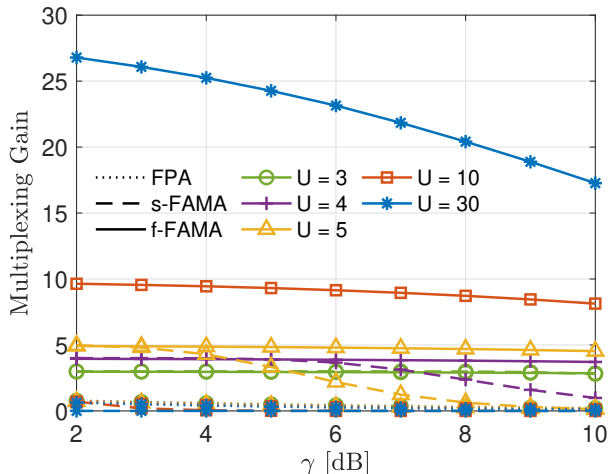


Fig. 7. The multiplexing gain for FAMA against the SINR threshold, γ , for different U , when $N = 20 \times 20$ and $W = 5\lambda \times 5\lambda$.

2) *Theoretical Performance*: Results in Fig. 7 are provided for the multiplexing gain of FAMA compared to FPA systems. It can be seen that the multiplexing gain decreases with the increasing SINR threshold, γ . The decrease of the multiplexing gain is more prominent with more users (i.e., with a higher U). *s-FAMA* provides higher multiplexing gain than FPA when the number of users, U , is relatively low. But when U increases, e.g., $U = 10$ or 30 , the multiplexing gain of *s-FAMA* decreases and approaches 0 because of too much interference. In contrast, *f-FAMA* provides considerable multiplexing gain even in the case of a high number of users, U .

3) *Link-level Simulation Results*: In [88], the link-level performance of *s-FAMA* with consideration of channel coding and OFDM was reported. Link-level simulation results in Fig. 8 are presented for the multiplexing gain of *s-FAMA* compared with FPA systems. The multiplexing gain in the link-level simulations is re-calculated as $m_{\text{FAMA}} = (1 - \text{BLER})U$, where BLER is the block error rate in the simulations. As we can see, *s-FAMA* provides great multiplexing gain in the low spectral efficiency region. The multiplexing gain decreases with increasing spectral efficiency. This is consistent with the theoretical performance in Fig. 7, since higher spectral efficiency requires higher SINR threshold γ . Specifically, when $U = 10$, *s-FAMA* can achieve multiplexing gain of 10 at a very low spectral efficiency, which is not achieved in Fig. 7. The reason is that the operating SINR is lower than $\gamma = 2$ dB and not presented in Fig. 7 for this low spectral efficiency.

4) *Variants of FAMA*: While considering the case of multiple activated ports, [84] proposed the CUMA scheme that processes the in-phase and quadrature parts of the received symbols individually. In CUMA, the activated ports can be chosen to add constructively to strengthen the desired signal. Thus, the classification of the ports can be performed as [84]

$$\left| \sum_{n \in \mathcal{N}^+} \text{real}(h_n^{(u,u)}) \right| \Bigg|_{\substack{\mathcal{N}^+ \\ \mathcal{N}^-}} \left| \sum_{n \in \mathcal{N}^-} \text{real}(h_n^{(u,u)}) \right|, \quad (42)$$

in which \mathcal{N}^+ denotes the set of port indices for all positive in-phase channels and \mathcal{N}^- for the negative in-phase channels.

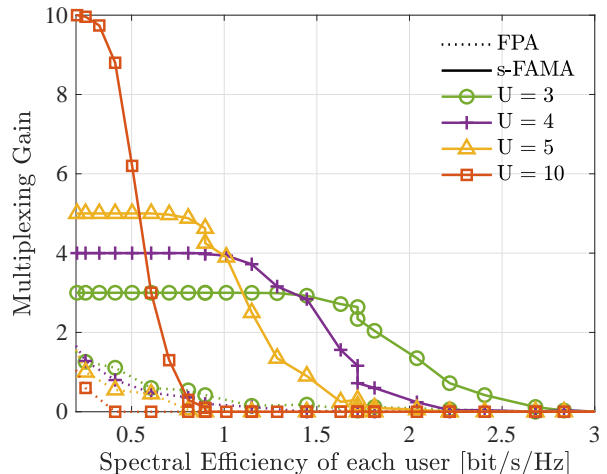


Fig. 8. The multiplexing gain for FAMA against the spectral efficiency of each users, when $N = 20 \times 20$ and $W = 5\lambda \times 5\lambda$.

With a predefined minimum required level of the in-phase channel to be on, ρ , the n -th port can be selected only if

$$\text{real}(h_n^{(u,u)}) \geq \rho \max_{m \in \mathcal{K}^s} \text{real}(h_m^{(u,u)}), \quad s \in \{+, -\}. \quad (43)$$

The final set, \mathcal{N} , can be obtained by choosing from \mathcal{N}^+ and \mathcal{N}^- using the criterion (42) but only those ports satisfying (43) is summed. Then, the in-phase and quadrant parts of the received symbol can be aggregated as [84]

$$\begin{cases} r_u^I = \sum_{k \in \mathcal{N}} \text{real}(r_n^{(u)}), \\ r_u^Q = \sum_{k \in \mathcal{N}} \text{imag}(r_n^{(u)}). \end{cases} \quad (44)$$

Finally, the received symbol is detected as [84]

$$\tilde{s}_u = \begin{bmatrix} \sum_{n \in \mathcal{N}} \text{real}(h_n^{(u,u)}) & - \sum_{n \in \mathcal{N}} \text{imag}(h_n^{(u,u)}) \\ \sum_{n \in \mathcal{N}} \text{imag}(h_n^{(u,u)}) & \sum_{n \in \mathcal{N}} \text{real}(h_n^{(u,u)}) \end{bmatrix} \times \begin{bmatrix} r_u^I \\ r_u^Q \end{bmatrix}. \quad (45)$$

The quality of detection can be further improved by repeating the above-mentioned process with focusing on the quadrature component. With the sophisticated selection of the ports, CUMA can support hundreds of users per channel use.

IV. NETWORKING TECHNOLOGY

While the foundational techniques of the physical layer establish the basis for FAS, networking techniques are equally essential for ensuring the efficient, reliable, and secure operation of practical implementations. Given that research on FAS is relatively recent, investigations into their upper layers remain in the preliminary stages. Nevertheless, the impact of networking techniques on the performance capabilities of FAS has increasingly garnered significant interest from both academic and industry sectors.

One of the primary objectives for networking technologies is the effective exploitation of radio resources. In this context, EE is considered as a critical performance metric. Moreover, it is essential to guarantee superior QoS within the constraints of limited radio resources. This section focuses on the QoS

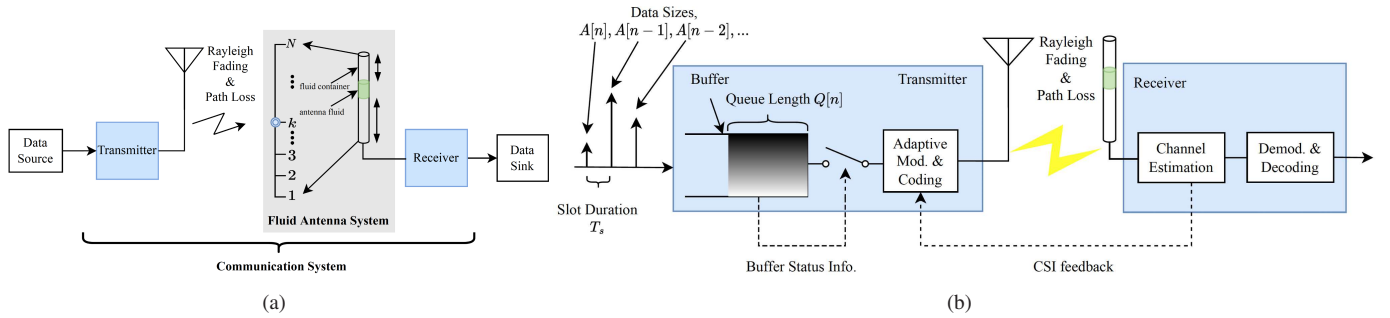


Fig. 9. The communication system model for a SISO-FAS: (a) a point-to-point channel model and (b) a discrete-time queueing model for FAS. Note that even a fluidic FAS is shown in practice, it could be realized using other technologies such as pixels and metamaterials.

enhancement in the FAS network, exploring power allocation strategies under QoS constraints, and studying content placement methodologies in content-centric FAS HetNets.

A. QoS Enhancement

Packet delay is one QoS metric considered in many wireless communication systems, such as 5G and 6G networks. For this reason, it is important to understand the statistical behavior of this delay in FAS. We discuss the key aspects below.

1) *QoS Modelling in Mobile Networks*: Fig. 9(a) depicts a simplified FAS-based point-to-point communication system model from an upper-layer data source to a data sink. With FAS installed at the receiver side, the received signal can be denoted as in (18), with the channel model specified in Section III-A. Moreover, the communication system inside the bracket of Fig. 9(a) is termed an FAS-based communication system; the details of such a system at slot n is shown in Fig. 9(b).

The communication system in Fig. 9(a) can be described as a discrete-time queueing model in Fig. 9(b). Let us denote the system bandwidth by B , the transmit power by P_t , and the noise spectral density by N_0 . This system is discrete-time; the slot duration is T_s . Provided that a path loss is L_p and the noise variance is given by $\sigma_\eta^2 = N_0 B$ [116], the average SNR, denoted by Γ , is defined as

$$\Gamma = \sigma^2 \frac{\mathbb{E}[|s|^2]}{\sigma_\eta^2} = \sigma^2 \frac{P_t}{N_0 B} \frac{L_p^{-1}}{\sigma^2} \rightarrow \frac{1}{L_p} \frac{P_t}{N_0 B} = \frac{P_t}{L_p \sigma_\eta}. \quad (46)$$

Upper-layer data from the data source are first pushed into a first-in-first-out (FIFO) buffer at the transmitter, and then transmitted to the receiver over a block-fading channel (i.e., the channel gains $\{g_k\}_{\forall k}$ remain constant during a time slot). Specifically, we define the following variables:

$A[n]$ for the amount of data in bits from the data source at time slot n . The RVs $A[1], A[2], \dots$ are assumed to be i.i.d. exponential random variables with its probability density function (PDF) being

$$f_A(a) = \begin{cases} \lambda \exp(-\lambda a) & \text{for } a \geq 0, \\ 0 & \text{for } a < 0. \end{cases} \quad (47)$$

The average data rate is $R = (T_s \lambda)^{-1}$ (bps);

$S[n]$ for the amount of data in bits that the transmitter is capable of transmitting at slot n . The random variables $S[1], S[2], \dots$ are i.i.d. from some fixed distribution;

$Q[n]$ for the backlog size in bits at slot n .

With the instantaneous channel gain h_{FAS} perfectly known at the transmitter side, the FAS-based system capacity C at slot n could be approximated as

$$C \approx B \log_2 \left(1 + \frac{h_{\text{FAS}} P_t}{N_0 B} \right) = B \log_2 \left(1 + \frac{h_{\text{FAS}} P_t}{\sigma_\eta^2} \right). \quad (48)$$

The capacity C and the service S have a simple relation

$$S = C T_s. \quad (49)$$

2) *Delay Distribution as QoS Metrics*: An analytical expression of delay distribution can be obtained by the use of the effective bandwidth and the effective capacity models. Because A is an exponential random variable with its PDF (47), the effective bandwidth of the arrival process is given by [117]

$$\alpha^{(b)}(u) = \frac{1}{T_s u} \log \left(\frac{\lambda}{\lambda - u} \right), \quad (50)$$

where u is the QoS exponent.

The PDF of the channel power gain g_{FAS} in an N -port FAS based on the simplified model (2) is given by

$$f_{h_{\text{FAS}}}(x) = \begin{cases} \frac{1}{\sigma^2} \exp\left(-\frac{x}{\sigma^2}\right), & N = 1 \\ \frac{N}{\sigma^2} \int_0^\infty F_X(x|r)^{N-1} f_X(x|r) e^{-\frac{x}{\sigma^2}} dr, & N > 1 \end{cases} \quad (51)$$

where

$$F_X(x|r) = 1 - Q_1 \left(\sqrt{\frac{\mu^2 r}{\sigma^2(1-\mu^2)}}, \sqrt{x} \right), \quad (52)$$

and

$$f_X(x|r) = \frac{1}{2} e^{-\frac{x + \frac{\mu^2 r}{\sigma^2(1-\mu^2)}}{2}} J_0 \left(\sqrt{\frac{\mu^2 h_0 x}{\sigma^2(1-\mu^2)}} \right). \quad (53)$$

Based on this PDF, the effective capacity is found as [117]

$$\begin{aligned} \alpha^{(c)}(u; P_t) &= \frac{-1}{T_s u} \log \int_0^\infty e^{-u T_s B \log_2(1 + x P_t / \sigma_\eta)} f_{h_{\text{FAS}}}(x) dx \\ &= \frac{-1}{T_s u} \log \int_0^\infty \left(1 + \frac{x P_t}{\sigma_\eta} \right)^{-\frac{u T_s B}{\log(2)}} f_{h_{\text{FAS}}}(x) dx. \end{aligned} \quad (54)$$

If the assumptions of the Gartner-Ellis theorem hold and if there is a unique QoS exponent $u^* > 0$ that satisfies

$$\alpha^{(b)}(u^*) = \alpha^{(c)}(u^*; P_t), \quad (55)$$

the complementary cumulative distribution function (CCDF) of delay can be accurately approximated by [117]

$$\begin{aligned} S_N(P_t; D_{\max}) &= \text{Prob}(D(\infty) > D_{\max}) \\ &\approx (1 - \lambda^{-1}u^*)^{D_{\max}+1}, \text{ for } D_{\max} \in \mathbb{N}_0, \end{aligned} \quad (56)$$

where \mathbb{N}_0 is a set of natural numbers including zero. Also, the expectation and variance of delay can be approximated as

$$\mathbb{E}[D(\infty)] = \frac{1 - \lambda^{-1}u^*}{\lambda^{-1}u^*} \quad (57)$$

and

$$\text{Var}[D(\infty)] = \frac{1 - \lambda^{-1}u^*}{(\lambda^{-1}u^*)^2}. \quad (58)$$

To illustrate the results, we simulate an N -port FAS with the path loss L_p based on the 3GPP model for a carrier frequency between 1400 MHz and 2600 MHz [118], defined as

$$L_p = 128.1 + 37.6 \log_{10}(d) + 21 \log_{10}\left(\frac{f_c}{2}\right), \quad (59)$$

where d denotes the distance between the transmitter and the receiver in km and f_c is the carrier frequency in GHz. In the simulations, we fix the distance d to 0.2 km, f_c to 2 GHz, the bandwidth to 10 MHz and the constant circuit power P_c to 0.1 Watts, the noise spectral density N_0 to -174 dBm/Hz and the slot duration to 1 ms.

Consider a 1D-FAS with $W = 1\lambda$, which is about 0.15 m. Given that the transmit power is 20 dBm and the average data rate R is 60 Mbps, we show the simulation and analytical results of the delay-outage probability (DOP) with respect to different values of the maximum delay bound D_{\max} in Fig. 10 when $N = 1, 5$ and 50. The x -axes are delay bounds (the unit is millisecond) and the y -axes are violation probabilities in log scale. Under any number of ports, the simulation result is obtained based on 10^6 samples of backlog size (1000 seconds ≈ 0.277 hours), the QoS exponent u^* is numerically found based on an algorithm in [117] and the analytical result is calculated by (56). As illustrated in Fig. 10, the simulation and analytical results almost overlap with each other in all three scenarios. This implies that (56) can accurately approximate the CCDF of delay in FASs with exponential arrival processes. On the other hand, the delay performance can be substantially improved by increasing the number of ports.

B. Power Allocation under QoS Constraints

Consider that the total transmission power can be expressed as $P_{\text{tot}} = P_c + P_t$, where P_c is the constant circuit power and P_t is the transmit power consumed by power amplifier. Based on Zorzi and Rao's definition in [119], an N -port FAS's EE can be found as

$$\eta_N(P_t) = \frac{R}{P_c + P_t}. \quad (60)$$

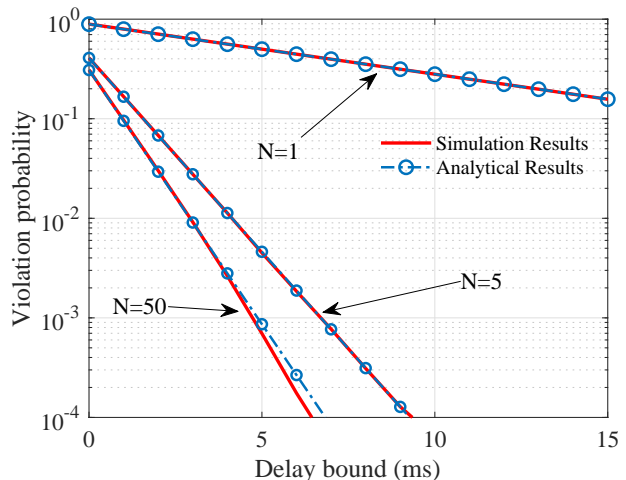


Fig. 10. Simulation and approximation results of $\text{Prob}(D > D_{\max})$.

As shown in Fig. 9(b), upper-layer data experience delays in a queueing buffer. We first define a maximum delay bound D_{\max} and a tolerance ϵ , and specify a target DOP constraint $\{D_{\max}, \epsilon\}$ in order to support QoS for a hypothetical application. The system has to guarantee the following inequality:

$$\text{Prob}(D(\infty) > D_{\max}) \leq \epsilon, \quad (61)$$

where $D(\infty)$ is the steady-state delay. Given that the transmitter decides the allocation of the transmit power P_t on the basis of the constraint $\{D_{\max}, \epsilon\}$ and the rest parameters are fixed, the EE can be optimized. That is to solve:

$$\begin{aligned} \max_{P_t \geq 0} \quad & \eta_N(P_t) \\ \text{s.t.} \quad & \text{Prob}(D(\infty) > D_{\max}) \leq \epsilon. \end{aligned} \quad (62)$$

Given the DOP constraint $\{D_{\max}, \epsilon\}$ and that the average packet length $1/\lambda$ at a slot is known, the target QoS exponent u^\dagger can be expressed as

$$u^\dagger = \lambda \left(1 - \epsilon^{\frac{1}{D_{\max}+1}} \right), \quad (63)$$

which is an inverse of the function (56) with respect to D_{\max} and ϵ . Moreover, the optimal power P_t^* is unique and satisfies the following equation:

$$\lambda \left(\int_0^\infty \left(1 + \frac{xP_t}{\sigma_\eta} \right)^{-\frac{u^\dagger T_c B}{\log(2)}} f_{g^*}(x; P_t) dx - 1 \right) = u^\dagger, \quad (64)$$

and P_t^* can be solved by any root-finding numerical methods, e.g., binary search method.

Consider again the same FAS with $W = 1\lambda$. In Fig. 11, we demonstrate numerical results on the maximum achievable EE obtained from (64) for different DOP constraints, i.e., $D_{\max} = \{0, 1, 2, \dots, 15\}$ ms where $\epsilon = 0.02$. We see that EE increases when extending D_{\max} and relaxing the DOP. When D_{\max} goes to infinity, the optimal transmit power converges a value that satisfies $R = \mathbb{E}[C]$, which is the condition for a stable system. Again, the EE in FAS-based communication systems is significantly higher compared with single-antenna FPA scenario. In the case of $D_{\max} = 1$ or 10 ms (required

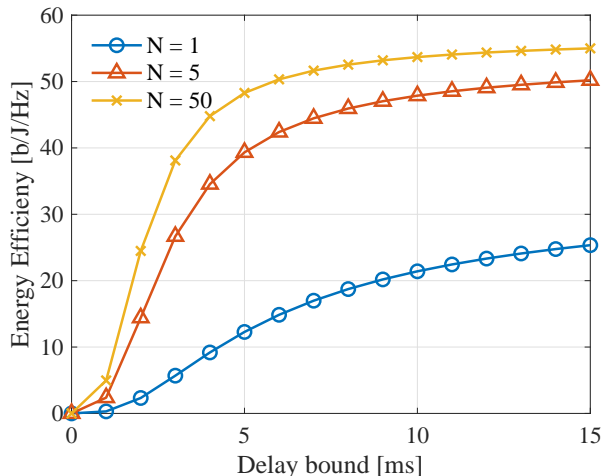


Fig. 11. Optimal EE under different DOP and number of ports of FAS.

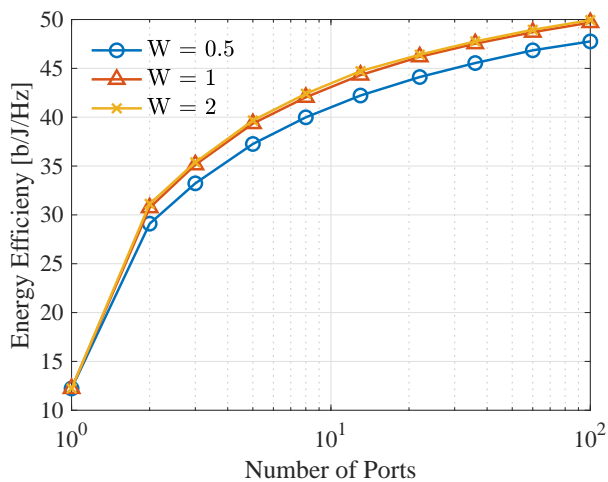


Fig. 12. Optimal EE using different number of ports of FAS and W under a DOP constraint $\{D_{\max} = 5 \text{ ms}, \epsilon = 0.02\}$.

for 5G/6G networks [120], respectively), the EE in a 50-port FAS is about 2.02 to 16.11 times higher than a FPA system.

Fig. 12 shows numerical results on the optimal EE under a target DOP constraint $\{D_{\max} = 5 \text{ ms}, \epsilon = 0.02\}$ using different number of ports, N , and different normalized size of FAS, W . The EE increases as N increases, but this growth becomes less pronounced when N is large. Additionally, it can be observed that increasing the size of FAS does enhance the EE of the systems, but the improvements are marginal.

C. Content Placement in Content-centric FAS HetNets

1) *Transmission Model and Content Placement:* As illustrated in Fig. 3, considering a multi-user CCN-enabled HetNet setup comprising SBSs tiers and 2D-FAS-equipped UEs. It is assumed that each SBS has limited storage and caches the most popular content. The UEs connect to their nearest SBS(s) that has the desired content, with a finite set of contents $\mathcal{F} := \{f_1, \dots, f_l, \dots, f_L\}$, where f_l is the l -th most popular content, while the SBSs connect to the backhaul via a macro-cell BS (MBS). The popularity of each content follows a Zipf

distribution, with the request probability for the l -th content given by [121]

$$p_l = \frac{l^{-\zeta}}{\sum_{k=1}^L k^{-\zeta}}, \quad (65)$$

in which ζ is the Zipf exponent and $\sum_{l=1}^L p_l = 1$. Each SBS can cache up to K contents, with $K \ll L$. Additionally, a probabilistic caching strategy is assumed, where each content is independently cached at each SBS with probability q_l . Thus, the set of caching probabilities $q = \{q_1, \dots, q_L\}$ must satisfy the constraint $\sum_{l=1}^L q_l \leq K$. It is also assumed that content is arranged in descending order of request probability, with more popular content being more likely to be cached.

A typical FAS-equipped UE with $N = N_1 \times N_2$ ports and size of $W = W_1 \lambda \times W_2 \lambda$ is located at the origin of a Cartesian plane, while the locations of SBSs are assumed to follow an independent homogeneous Poisson point process (HPPP) Ψ^S with intensity μ_S . Specifically, the point process Ψ_l^S represents the SBSs that cache content l , with intensity $q_l \mu_S$ in each tier. The intensity of UEs is assumed to be much higher than that of SBSs, and each FAS-equipped UE is allowed to communicate with one SBS per time slot. Therefore, the received SNR at a FAS-equipped UE requesting content l from its respective SBS that includes this content is defined as

$$\gamma_l = \frac{P_t |h_{n^*}^{(l)}|^2 D(|X_l|)}{\sigma_\eta^2}, \quad (66)$$

where P_t denotes the transmit power, and $D(|X_l|) = \beta |X_l|^{-\alpha}$ represents the path-loss with the distance $|X_l|$, in which β and α are the frequency-dependent constant and the path-loss exponent, respectively. Under the assumption of advanced interference management algorithms, communications are noise-limited, and inter-cell interference is relatively low, so σ_η^2 in (66) represents the combined power of noise and weak interference at the FAS-equipped UE. Additionally, n^* is the index of the best port, given by

$$n^* = \arg \max_n \left\{ |h_n^{(l)}|^2 \right\}, \quad (67)$$

where $h_n^{(l)}$ is the channel coefficient between the n -th port of a typical FAS-equipped UE and its serving SBS, and the channel gain $g_n^{(l)} = |h_n^{(l)}|^2$ follows exponential distribution, i.e., $g_n^{(l)} \sim \text{Exp}(1)$. According to (67), we have

$$g_{\text{FAS}}^{(l)} = g_{n^*}^{(l)} = \max \left\{ g_1^{(l)}, \dots, g_N^{(l)} \right\}. \quad (68)$$

By assuming a 3D environment under rich scattering, the covariance $J_{k,l}$ between two arbitrary ports k and l is characterized as (8). Note that in the FAS-equipped UEs only the optimal port that maximizes the received SNR is activated. Hence, as shown in [122], the covariance of Jakes' model $J_{k,l}$ is effectively approximated with the dependence parameter ϑ of elliptical copulas, e.g., the Gaussian copula, the cumulative density function (CDF) of $g_{\text{FAS}}^{(l)}$ is given by [122]

$$F_{g_{\text{FAS}}^{(l)}}(r) = \Phi_{\mathbf{R}} \left(\phi^{-1} \left(F_{g_1^{(l)}}(r) \right), \dots, \phi^{-1} \left(F_{g_N^{(l)}}(r) \right); \vartheta \right), \quad (69)$$

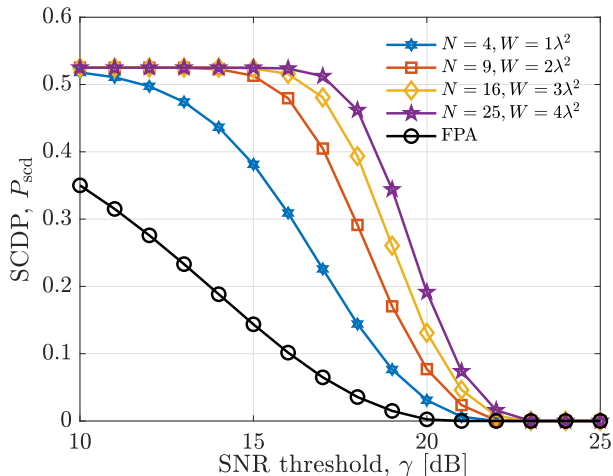


Fig. 13. SCDP versus threshold γ when $q_l = 1$.

where $\Phi_{\mathbf{R}}$ is the joint CDF of a multivariate normal distribution with mean zero and correlation matrix \mathbf{R} , and $\phi^{-1}(x) = \sqrt{2}\text{erf}^{-1}(2x - 1)$ is the quantile function of the standard normal distribution, in which $\text{erf}^{-1}(\cdot)$ refers to the inverse error function and $F_{g_k^{(v)}}(r) = 1 - e^{-r}$.

2) *Performance Analysis:* The performance of content delivery systems is crucial for optimizing network efficiency. Two key performance metrics that are essential for analyzing the performance of CCN are the successful content delivery probability (SCDP) and the content delivery delay (CDD). The SCDP quantifies the likelihood that a content requested by a typical UE is both cached within the network and successfully transmitted, providing an indication of the system's efficiency in meeting user demands. On the other hand, CDD measures the delay associated with delivering content to the UE, taking into account retransmission protocols such as automatic repeat request (ARQ) and the impact of channel fading.

a) *SCDP:* For downlink, the SCDP is mathematically defined as $P_{\text{scd}} = \sum_{l=1}^L p_l P_{s,l}$, where the probability of successful transmission is calculated as $P_{s,l} = \text{Prob}(\gamma_l \geq \gamma)$, and γ represents the SNR threshold. Given that $P_{s,l}$ is conditioned on the random variable $|X_l|$, which represents the distance between the typical FAS-equipped UE and its nearest serving SBS that has cached content l , P_{scd} is reformulated as

$$\begin{aligned} P_{\text{scd}} &= \sum_{l=1}^L p_l \mathbb{E}_{|X_l|} \left\{ \text{Prob} \left(\gamma_l \geq \gamma \mid |X_l| = x \right) \right\} \\ &= \sum_{l=1}^L p_l \int_0^\infty \text{Prob}(\gamma_l \geq \gamma) f_{|X_l|}(x) dx, \end{aligned} \quad (70)$$

where $f_{|X_l|}(x)$ is the PDF of $|X_l|$, given by [121]

$$f_{|X_l|}(x) = 2\pi q_l \mu_S x \exp(-\pi q_l \mu_S x^2). \quad (71)$$

Therefore, the SCDP can be derived as

$$P_{\text{scd}} = \sum_{l=1}^L p_l \underbrace{2\pi \mu_S q_l \int_0^\infty \left[1 - F_{g_{\text{FAS}}^{(v)}} \left(\frac{\gamma \sigma_\eta^2}{P\beta} x^\alpha \right) \right] x e^{-\pi q_l \mu_S x^2} dx}_{P_{s,l}}. \quad (72)$$

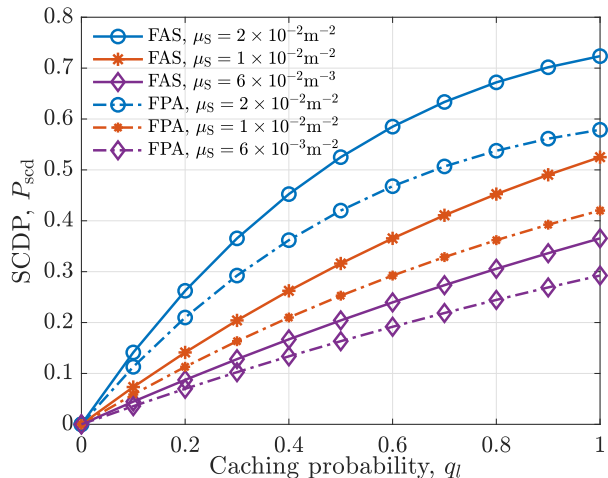


Fig. 14. SCDP versus caching probability q_l when $N = 3 \times 3$, $W = 1\lambda \times 1\lambda$.

Solving the integral (72) is mathematically intractable but it can be solved numerically. By setting the simulation parameters as $L = 100$, $K = 10$, $A = 4$, $\mu_S = 10^{-2} \text{ m}^{-2}$, $P = -30 \text{ dBm}$, $\sigma^2 = -60 \text{ dBm}$, $\alpha = 3$, $\beta = 1$, $\gamma = 0 \text{ dB}$, $\zeta = 1$, and $T_0 = 1 \text{ ms}$, the SCDP and CDD are analyzed by the results in Figs. 13 and 14 for various scenarios.

Fig. 13 illustrates the impact of the SNR threshold γ on the SCDP for W and N , considering the scenario in which the caching placement probability is $q_l = 1$. It can be seen that compared to the FPA system, deploying an FAS at the UE significantly enhances transmission reliability. Moreover, simultaneously increasing both W and N improves the SCDP, as it balances the spatial correlation between antenna ports while enhancing channel capacity, diversity gain, and spatial multiplexing. Fig. 14 illustrates the impact of FAS deployment on caching placement. The results show that SCDP increases monotonically with q_l for both FAS and FPA, as higher caching probability enhances content accessibility. Moreover, increasing μ_S improves SCDP by reducing the distance between UEs and their serving SBSs, thereby enhancing overall SNR. Interestingly, these improvements are significantly more pronounced with FAS deployment than with FPA.

b) *CDD:* The ARQ-based protocol is considered, where an FAS-equipped UE requests content from the nearest SBS, which retransmits up to M times until successful delivery. Upon success, the SBS receives a one-bit acknowledgment; otherwise, a negative acknowledgment is sent. Each ARQ round lasts T_0 , and an outage occurs if delivery fails after M attempts. Thus, the CDD is mathematically obtained as

$$\begin{aligned} D_{\text{cd}} &= T_0 + T_0(1 - P_{s,l}) + \dots + T_0(1 - P_{s,l})^{M-1} \\ &= T_0 \frac{1 - (1 - P_{s,l})^M}{P_{s,l}}, \end{aligned} \quad (73)$$

where $P_{s,l}$ has been defined in (72). Moreover, by considering the high ARQ rounds regime, i.e., $M \rightarrow \infty$, the CDD in (73) can be derived as $D_{\text{cd}}^\infty = T_0/P_{s,l}$.

Fig. 15 highlights the impact of FAS on CDD under varying SNR thresholds. FAS-equipped UEs experience significantly lower delays compared to FPA-based UEs. For instance, at

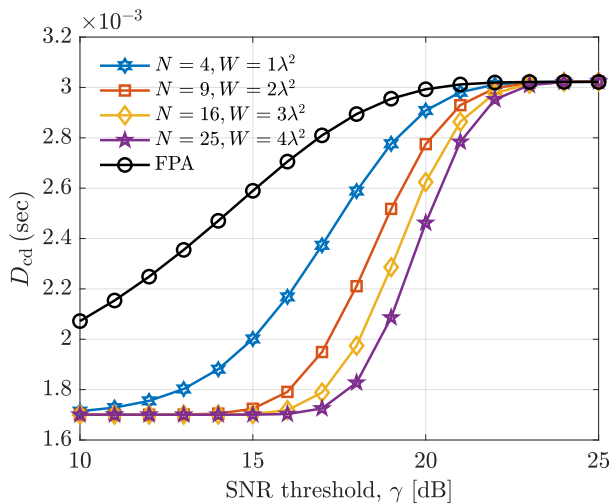


Fig. 15. CDD versus SNR threshold γ when $q_l = 1$ and $M = 3$.

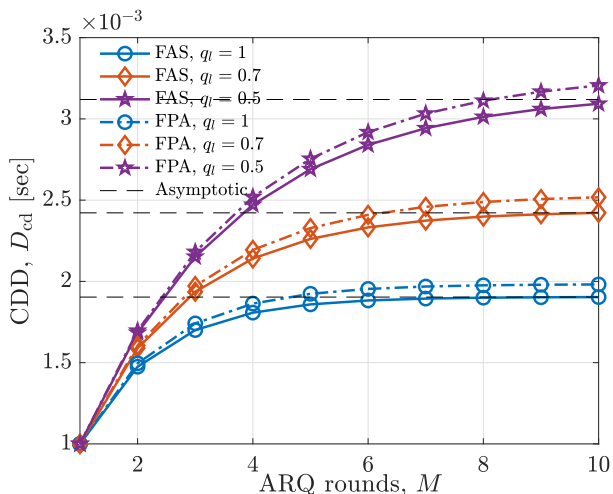


Fig. 16. CDD versus ARQ rounds M when $N = 3 \times 3$, $W = 1\lambda \times 1\lambda$.

$\gamma = 15$ dB, a UE with FAS ($N = 3 \times 3$, $W = \sqrt{2}\lambda \times \sqrt{2}\lambda$) achieves a CDD of approximately 1.72 ms, while a FPA-based UE faces a delay of about 2.6 ms, representing a reduction of 33.85%. Fig. 16 examines the effect of M on CDD. As M increases, delays rise due to more retransmission attempts. Additionally, lower caching probability results in higher delays, as the likelihood of the requested content being available at the nearest SBS decreases. Notably, FAS deployment consistently outperforms FPA system in these scenarios, delivering content with lower delays, even as M and q_l fluctuate.

V. CHALLENGES AND OPEN ISSUES

The investigation into FAS has stimulated strong research interest. However, substantial efforts are required to facilitate the practical application of FAS. Based on our prior discussions, the following challenges and open issues lie ahead.

A. System Modeling and Electromagnetic Compliance

FAS necessitates precise electromagnetic models to accommodate dynamic changes in shape, position, material and other

properties. Existing models struggle to achieve an appropriate balance between computational complexity and real-world accuracy. Moreover, the increasing operating frequencies necessitate the adoption of a near-field model. Therefore, it is imperative to explore accurate models for FAS's ultra-high spatial resolution in both far-field and near-field contexts.

B. Channel Estimation and Management

The dynamic reconfiguration of FAS mandates continuous channel estimation, increasing overhead in densely populated networks. Advanced technologies such as AI and machine learning approaches can potentially minimize the required channel acquisitions. Nonetheless, the number of observation ports required to accurately recover the CSI for large-scale configurations remains high. The ongoing reduction of CSI overhead without compromising performance continues to be a significant concern to reveal the capability of FAS.

C. Hardware limitations

The state-of-the-art channel models for FAS mainly emphasize theoretical frameworks, with empirical channel models remaining notably scarce. The development of an empirical channel model necessitates numerous channel measurements, a process that hinges on the maturity of FAS hardware. Current FAS devices remains in its infancy, with existing prototypes inadequately developed for practical applications, thereby facing durability and miniaturization issues.

D. Green FAS

Given the rising carbon emissions resulting from excessive power consumption in wireless communication networks. EE has become a critical performance metric for future wireless infrastructures. However, the evaluation on the EE in FAS focuses on single-cell environment. Furthermore, current models consider circuit power as constant, while dynamic reconfiguration of FAS may lead to increased power demands. Consequently, a thorough analysis of the realistic EE performance of FAS is warranted, taking into account detailed circuit power dynamics in multi-cell scenarios.

E. Security and Privacy

The reconfigurability of FAS may introduce new vulnerability, including potential scenarios for beam-hijacking attacks. Robust encryption methodologies and dynamic beam-nulling techniques are still in the development stages. Furthermore, the spatial adaptability of FAS may inadvertently expose user location data, requiring anonymization frameworks. The physical layer vulnerability and the privacy issue beyond FAS need careful treatment and further investigations.

F. Standardization and Deployment

The high costs associated with the development of FAS infrastructure present a significant challenge. Should FAS be employed at the transmitter side to enhance DoF, necessary modifications to the feedback channel will be required. Nevertheless, as the integration of more antenna ports and efficient

MIMO remains a focal topic of standardization, FAS presents a promising solution to satisfy these requirements contingent upon appropriate design considerations.

G. New Application Scenarios

The introduction of FAS is driving rapid transformations within wireless networks. Due to its extensive DoF, it can be integrated into various emerging technologies to further enhance performance. For instance, FAS-enabled edge networks may improve transmission rates from the edge devices to servers, thereby improving computational capabilities. Numerous opportunities exist in new scenarios that extend beyond the scope of this discussion. Thorough investigation in the future will be crucial for the maturation of this technology.

VI. CONCLUSION

This paper provided a contemporary survey on the pertinent subject of FAS, encompassing key application scenarios, fundamental physical-layer techniques, and relevant networking technologies. The application scenarios were categorized into three principal types: single-user HomoNet, multi-user HomoNet, and HetNets. Subsequently, the fundamental aspects of FAS were presented, with particular focus on channel modeling and channel estimation as crucial components for understanding FAS behavior. The paper further summarized transmission models, theoretical analyses, link-level simulation results, and their variants for both single-user FAS and multi-user FAMA. At the time of this writing, there is growing interest in associated networking solutions. To this end, the discussion included techniques for QoS enhancement in FAS networks and strategies for power allocation under QoS constraints. In addition, this paper addressed content placement strategies in FAS-based HetNets, which can improve system efficiency by reducing delivery delays. Further research into networking techniques for FAS can be pursued from multiple perspectives. In summary, this marks an exciting period for researchers engaged in the study of FAS.

REFERENCES

- [1] H. Tataria *et al.*, “6G wireless systems: Vision, requirements, challenges, insights, and opportunities,” *Proc. IEEE*, vol. 109, no. 7, pp. 1166–1199, July 2021.
- [2] N. Rajatheva *et al.*, “White paper on broadband connectivity in 6G,” *arXiv preprint, arXiv:2004.14247*, 2020.
- [3] W. Saad, M. Bennis and M. Chen, “A vision of 6G wireless systems: Applications, trends, technologies, and open research problems,” *IEEE Network*, vol. 34, no. 3, pp. 134–142, May/June 2020.
- [4] F. Tariq *et al.*, “A speculative study on 6G,” *IEEE Wireless Commun.*, vol. 27, no. 4, pp. 118–125, Aug. 2020.
- [5] P. Wang, J. Xiao and L. Ping, “Comparison of orthogonal and non-orthogonal approaches to future wireless cellular systems,” *IEEE Veh. Technol. Mag.*, vol. 1, no. 3, pp. 4–11, Sept. 2006.
- [6] Y. Saito *et al.*, “Non-orthogonal multiple access (NOMA) for cellular future radio access,” in *Proc. IEEE Veh. Technol. Conf. (VTC Spring)*, pp. 1–5, 2–5 Jun. 2013, Dresden, Germany.
- [7] L. Dai *et al.*, “Non-orthogonal multiple access for 5G: Solutions, challenges, opportunities, and future research trends,” *IEEE Commun. Mag.*, vol. 53, no. 9, pp. 74–81, Sept. 2015.
- [8] Z. Lin *et al.*, “Supporting IoT with rate-splitting multiple access in satellite and aerial-integrated networks,” *IEEE Int. Things J.*, vol. 8, no. 14, pp. 11123–11134, Jul. 2021.
- [9] Y. Mao *et al.*, “Rate-splitting multiple access: Fundamentals, survey, and future research trends,” *IEEE Commun. Surv. & Tut.*, vol. 24, no. 4, pp. 2073–2126, Apr. 2022.
- [10] Z. Wang *et al.*, “Extremely large-scale MIMO: Fundamentals, challenges, solutions, and future directions,” *IEEE Wireless Commun.*, vol. 31, no. 3, pp. 117–124, Jun. 2024.
- [11] M. Rowshan, M. Qiu, Y. Xie, X. Gu and J. Yuan, “Channel coding toward 6G: Technical overview and outlook,” *IEEE open j. Commun. Soc.*, vol. 5, pp. 2585–2685, Apr. 2024.
- [12] H. Hong *et al.*, “Enhanced nonuniform constellations for high-capacity communications with low-complexity demappers,” *IEEE Trans. Broadcast.*, vol. 68, no. 3, pp. 740–752, Sept. 2022.
- [13] Y. Li, F. Zhou, L. Yuan, Q. Wu and N. Al-Dhahir, “Cognitive semantic communication: A new communication paradigm for 6G,” *IEEE Commun. Mag.*, vol. 63, no. 6, pp. 122–129, Jun. 2025.
- [14] G. C. Alexandropoulos *et al.*, “Reconfigurable intelligent surfaces for rich scattering wireless communications: Recent experiments, challenges, and opportunities,” *IEEE Commun. Mag.*, vol. 59, no. 6, pp. 28–34, 2021.
- [15] M. Jian *et al.*, “Reconfigurable intelligent surfaces for wireless communications: Overview of hardware designs, channel models, and estimation techniques,” *Intelligent & Conv. Netw.*, vol. 3, no. 1, pp. 1–32, 2022.
- [16] E. Basar *et al.*, “Reconfigurable intelligent surfaces for 6G: Emerging applications and open challenges,” *IEEE Veh. Technol. Mag.*, vol. 19, no. 3, pp. 27–47, 2024.
- [17] K. B. Letaief *et al.*, “The roadmap to 6G: AI empowered wireless networks,” *IEEE Commun. Mag.*, vol. 57, no. 8, pp. 84–90, Aug. 2019.
- [18] C.-X. Wang *et al.*, “Artificial intelligence enabled wireless networking for 5G and beyond: Recent advances and future challenges,” *IEEE Wireless Commun.*, vol. 27, no. 1, pp. 16–23, Feb. 2020.
- [19] L. Song *et al.*, “Networking systems of AI: On the convergence of computing and communications,” *IEEE Internet Things J.*, vol. 9, no. 20, pp. 20352–20381, Oct. 2022.
- [20] I. F. Akyildiz *et al.*, “Terahertz band communication: An old problem revisited and research directions for the next decade,” *IEEE Trans. Commun.*, vol. 70, no. 6, pp. 4250–4285, Jun. 2022.
- [21] C. Chaccour *et al.*, “Seven defining features of terahertz (THz) wireless systems: A fellowship of communication and sensing,” *IEEE Commun. Surv. Tuts.*, vol. 24, no. 2, pp. 967–993, 2nd Quart. 2022.
- [22] W. Jiang *et al.*, “Terahertz communications and sensing for 6G and beyond: A comprehensive review,” *IEEE Commun. Surv. Tuts.*, vol. 26, no. 4, pp. 2326–2381, 4th Quart. 2024.
- [23] G. Araniti, A. Iera, S. Pizzi and F. Rinaldi, “Toward 6G non-terrestrial networks,” *IEEE Network*, vol. 36, no. 1, pp. 113–120, Jan./Feb. 2022.
- [24] S. Mahboob and L. Liu, “Revolutionizing future connectivity: A contemporary survey on AI-empowered satellite-based non-terrestrial networks in 6G,” *IEEE Commun. Surv. Tuts.*, vol. 26, no. 2, pp. 1279–1321, 2nd Quart. 2024.
- [25] F. Liu *et al.*, “Integrated sensing and communications: Toward dual-functional wireless networks for 6G and beyond,” *IEEE J. Sel. Areas Commun.*, vol. 40, no. 6, pp. 1728–1767, Jun. 2022.
- [26] A. Liu *et al.*, “A survey on fundamental limits of integrated sensing and communication,” *IEEE Commun. Surv. Tuts.*, vol. 24, no. 2, pp. 994–1034, 2nd Quart. 2022.
- [27] S. Lu *et al.*, “Integrated sensing and communications: Recent advances and ten open challenges,” *IEEE Internet Things J.*, vol. 11, no. 11, pp. 19094–19120, Jun. 2024.
- [28] K.-K. Wong, K.-F. Tong, Y. Zhang, and Z. Zheng, “Fluid antenna system for 6G: When Bruce Lee inspires wireless communications,” *Elect. Lett.*, vol. 56, no. 24, pp. 1288–1290, Nov. 2020.
- [29] K.-K. Wong, K.-F. Tong, Y. Shen, Y. Chen, and Y. Zhang, “Bruce Lee-inspired fluid antenna system: Six research topics and the potentials for 6G,” *Frontiers Commun. Netw.*, vol. 3, Mar. 2022, Art. no. 853416.
- [30] K. K. Wong, A. Shojaefard, K. F. Tong, and Y. Zhang, “Performance limits of fluid antenna systems,” *IEEE Commun. Lett.*, vol. 24, no. 11, pp. 2469–2472, Nov. 2020.
- [31] K. K. Wong, A. Shojaefard, K. F. Tong, and Y. Zhang, “Fluid antenna systems,” *IEEE Trans. Wireless Commun.*, vol. 20, no. 3, pp. 1950–1962, Mar. 2021.
- [32] Y. Huang *et al.*, “Liquid antennas: Past, present and future,” *IEEE Open J. Antennas & Propag.*, vol. 2, pp. 473–487, Mar. 2021.
- [33] K. N. Paracha *et al.*, “Liquid metal antennas: Materials, fabrication and applications,” *Sensors*, vol. 20, no. 1, p. 177, Dec. 2019.
- [34] Y. Shen *et al.*, “Design and implementation of mmWave surface wave enabled fluid antennas and experimental results for fluid antenna multiple access,” *arXiv preprint, arXiv:2405.09663*, May 2024.

- [35] T. V. Hoang *et al.*, “Computational polarimetric imaging using two-dimensional dynamic metasurface apertures,” *IEEE Open J. Antennas & Propag.*, vol. 2, pp. 488–497, Mar. 2021.
- [36] J. Zhang *et al.*, “A novel pixel-based reconfigurable antenna applied in fluid antenna systems with high switching speed,” *IEEE Open J. Antennas & Propag.*, vol. 6, no. 1, pp. 212–228, Feb. 2025.
- [37] S. Basbug, “Design and synthesis of antenna array with movable elements along semicircular paths,” *IEEE Antennas Wireless Propag. Lett.*, vol. 16, pp. 3059–3062, Oct. 2017.
- [38] M. C. Johnson, S. L. Brunton, N. B. Kundtz, and J. N. Kutz, “Sidelobe canceling for reconfigurable holographic metamaterial antenna,” *IEEE Trans. Antennas & Propag.*, vol. 63, no. 4, pp. 1881–1886, Apr. 2015.
- [39] R. Deng *et al.*, “Reconfigurable holographic surfaces for ultra-massive MIMO in 6G: Practical design, optimization and implementation,” *IEEE J. Select. Areas Commun.*, vol. 41, no. 8, pp. 2367–2379, Aug. 2023.
- [40] B. Liu, K. F. Tong, K. K. Wong, C.-B. Chae, and H. Wong, “Be water, my antennas: Riding on radio wave fluctuation in nature for spatial multiplexing using programmable meta-fluid antenna,” *arXiv preprint, arXiv:2502.04693*, 2025.
- [41] L. Zhu, and K. K. Wong, “Historical review of fluid antennas and movable antennas,” *arXiv preprint, arXiv:2401.02362v2*, Jan. 2024.
- [42] A. Fukuda, H. Yamamoto, H. Okazaki, Y. Suzuki, and K. Kawai, “Pinching antenna: Using a dielectric waveguide as an antenna,” *NTT DOCOMO Tech. J.*, vol. 23, no. 3, pp. 5–12, Jan. 2022.
- [43] K. K. Wong, K. F. Tong, Z. Chu, and Y. Zhang, “A vision to smart radio environment: Surface wave communication superhighways,” *IEEE Wireless Commun.*, vol. 28, no. 1, pp. 112–119, Feb. 2021.
- [44] B. Cetiner *et al.*, “Multifunctional reconfigurable MEMS integrated antennas for adaptive MIMO systems,” *IEEE Commun. Mag.*, vol. 42, no. 12, pp. 62–70, Dec. 2004.
- [45] F. Fazel, A. Grau, H. Jafarkhani and F. De Flaviis, “State-selection in a space-time-state block coded MIMO communication system using reconfigurable pixel antennas,” in *Proc. IEEE Global Telecommun. Conf.*, Dec. 2008, pp. 1–5.
- [46] A. M. Sayeed and V. Raghavan, “Maximizing MIMO capacity in sparse multipath with reconfigurable antenna arrays,” *IEEE J. Select. Topics Sig. Process.*, vol. 1, no. 1, pp. 156–166, Jun. 2007.
- [47] A. Shojaeifard *et al.*, “MIMO evolution beyond 5G through reconfigurable intelligent surfaces and fluid antenna systems,” *Proc. IEEE*, vol. 110, no. 9, pp. 1244–1265, Sept. 2022.
- [48] K.-K. Wong *et al.*, “Fluid antenna system—part I: Preliminaries,” *IEEE Commun. Lett.*, vol. 27, no. 8, pp. 1919–1923, Aug. 2023.
- [49] K.-K. Wong, K.-F. Tong, and C.-B. Chae, “Fluid antenna system—part II: Research opportunities,” *IEEE Commun. Lett.*, vol. 27, no. 8, pp. 1924–1928, Aug. 2023.
- [50] K.-K. Wong, K.-F. Tong, and C.-B. Chae, “Fluid antenna system—part III: A new paradigm of distributed artificial scattering surfaces for massive connectivity,” *IEEE Commun. Lett.*, vol. 27, no. 8, pp. 1929–1933, Aug. 2023.
- [51] A. F. M. S. Shah *et al.*, “A survey on fluid antenna multiple access for 6G: A new multiple access technology that provides great diversity in a small space,” *IEEE Access*, vol. 12, pp. 88410–88425, 2024.
- [52] W. K. New *et al.*, “A tutorial on fluid antenna system for 6G networks: Encompassing communication theory, optimization methods and hardware designs,” *IEEE Commun. Surv. Tuts.*, early access, doi:10.1109/COMST.2024.3498855, 2024.
- [53] W.-J. Lu *et al.*, “Fluid antennas: Reshaping intrinsic properties for flexible radiation characteristics in intelligent wireless networks,” *IEEE Commun. Mag.*, vol. 63, no. 5, pp. 40–45, May 2025.
- [54] Z. Chai, K. K. Wong, K. F. Tong, Y. Chen and Y. Zhang, “Port selection for fluid antenna systems,” *IEEE Commun. Lett.*, vol. 26, no. 5, pp. 1180–1184, May 2022.
- [55] W. K. New, K. K. Wong, H. Xu, K. F. Tong and C. B. Chae, “Fluid antenna system: New insights on outage probability and diversity gain,” *IEEE Trans. Wireless Commun.*, vol. 23, no. 1, pp. 128–140, Jan. 2024.
- [56] F. Rostami Ghadi, M. Kaveh, K.-K. Wong and Y. Zhang, “Performance analysis of FAS-aided backscatter communications,” *IEEE Wireless Commun. Lett.*, vol. 13, no. 9, pp. 2412–2416, Sept. 2024.
- [57] F. Rostami Ghadi *et al.*, “Physical layer security over fluid antenna systems: Secrecy performance analysis,” *IEEE Trans. Wireless Commun.*, vol. 23, no. 12, pp. 18201–18213, Dec. 2024.
- [58] W. K. New, K.-K. Wong, H. Xu, K.-F. Tong and C.-B. Chae, “An information-theoretic characterization of MIMO-FAS: Optimization, diversity-multiplexing tradeoff and q -outage capacity,” *IEEE Trans. Wireless Commun.*, vol. 23, no. 6, pp. 5541–5556, Jun. 2024.
- [59] Y. Ye *et al.*, “Fluid antenna-assisted MIMO transmission exploiting statistical CSI,” *IEEE Commun. Lett.*, vol. 28, no. 1, pp. 223–227, Jan. 2024.
- [60] I. Krikidis *et al.*, “Optimizing configuration selection in reconfigurable-antenna MIMO systems: Physics-inspired heuristic solvers,” *IEEE Trans. Commun.*, vol. 72, no. 12, pp. 8010–8023, Dec. 2024.
- [61] C. N. Efreem and I. Krikidis, “Transmit and receive antenna port selection for channel capacity maximization in fluid-MIMO systems,” *IEEE Wireless Commun. Lett.*, vol. 13, no. 11, pp. 3202–3206, Nov. 2024.
- [62] F. Rostami Ghadi *et al.*, “On performance of RIS-aided fluid antenna systems,” *IEEE Wireless Commun. Lett.*, vol. 13, no. 8, pp. 2175–2179, Aug. 2024.
- [63] X. Lai *et al.*, “FAS-RIS: A block-correlation model analysis,” *IEEE Trans. Veh. Technol.*, vol. 74, no. 2, pp. 3412–3417, Feb. 2025.
- [64] J. Yao *et al.*, “FAS-RIS communication: Model, analysis, and optimization,” *IEEE Trans. Veh. Technol.*, early access, doi:10.1109/TVT.2025.3537294, Jan. 2025.
- [65] J. Yao *et al.*, “A framework of FAS-RIS systems: Performance analysis and throughput optimization,” *arXiv preprint, arxiv:2407.08141*, 2024.
- [66] J. Chen *et al.*, “Low-complexity beamforming design for RIS-assisted fluid antenna systems,” *Proc. IEEE Int. Conf. Commun. Workshops (ICC Workshops)*, pp. 1377–1382, 9–13 Jun. 2024, Denver, CO, USA.
- [67] F. Rostami Ghadi *et al.*, “Secrecy performance analysis of RIS-aided fluid antenna systems,” *2025 IEEE Wireless Commun. Network. Conf. (WCNC)*, pp. 1–6, Mar. 2025, Milan, Italy.
- [68] F. Rostami Ghadi *et al.*, “Phase-mismatched STAR-RIS with FAS-assisted RSMA users,” *arXiv preprint, arxiv:2503.08986*, Mar. 2025.
- [69] E. Faddoul *et al.*, “Correlation mitigation schemes for index-modulated fluid antenna systems,” *Proc. IEEE Global Commun. Conf. (GLOBECOM)*, Kuala Lumpur, Malaysia, Feb. 2023, pp. 5324–5329.
- [70] H. Yang *et al.*, “Position index modulation for fluid antenna system,” *IEEE Trans. Wireless Commun.*, vol. 23, no. 11, pp. 16773–16787, Nov. 2024.
- [71] J. Zhu *et al.*, “Index modulation for fluid antenna-assisted MIMO communications: System design and performance analysis,” *IEEE Trans. Wireless Commun.*, vol. 23, no. 8, pp. 9701–9713, Aug. 2024.
- [72] X. Guo *et al.*, “Fluid antenna index modulation for MIMO systems: Robust transmission and low-complexity detection,” *arXiv preprint, arxiv:2412.04877*, 2024.
- [73] Y. Chen, H. Xu and T. Xu, “Enhancing communication resilience through fluid antenna index modulation,” *Proc. IEEE/CIC Int. Conf. Commun. China (ICCC)*, Hangzhou, China, Sep. 2024, pp. 1304–1309.
- [74] Y. Chen and T. Xu, “Fluid antenna index modulation communications,” *IEEE Wireless Commun. Lett.*, vol. 13, no. 4, pp. 1203–1207, Apr. 2024.
- [75] J. Zhu *et al.*, “Fluid antenna empowered index modulation for RIS-aided mmWave transmissions,” *IEEE Trans. Wireless Commun.*, vol. 24, no. 2, pp. 1635–1647, Feb. 2025.
- [76] J. Yao *et al.*, “Rethinking hardware impairments in multi-user systems: Can FAS make a difference?,” *arXiv preprint, arxiv:2412.15843*, 2024.
- [77] H. Xu *et al.*, “Channel estimation for FAS-assisted multiuser mmWave systems,” *IEEE Commun. Lett.*, vol. 28, no. 3, pp. 632–636, Mar. 2024.
- [78] H. Xu *et al.*, “Capacity maximization for FAS-assisted multiple access channels,” *IEEE Trans. Commun.*, early access, doi:10.1109/TCOMM.2024.3516499, Dec. 2024.
- [79] K. K. Wong and K. F. Tong, “Fluid antenna multiple access,” *IEEE Trans. Wireless Commun.*, vol. 21, no. 7, pp. 4801–4815, Jul. 2022.
- [80] K. K. Wong, K. F. Tong, Y. Chen, and Y. Zhang, “Fast fluid antenna multiple access enabling massive connectivity,” *IEEE Commun. Lett.*, vol. 27, no. 2, pp. 711–715, Feb. 2023.
- [81] K.-K. Wong *et al.*, “Slow fluid antenna multiple access,” *IEEE Trans. Commun.*, vol. 71, no. 5, pp. 2831–2846, May 2023.
- [82] P. Ramírez-Espinosa, D. Morales-Jimenez and K. K. Wong, “A new spatial block-correlation model for fluid antenna systems,” *IEEE Trans. Wireless Commun.*, vol. 23, no. 11, pp. 15829–15843, Nov. 2024.
- [83] H. Xu *et al.*, “Revisiting outage probability analysis for two-user fluid antenna multiple access system,” *IEEE Trans. Wireless Commun.*, vol. 23, no. 8, pp. 9534–9548, Aug. 2024.
- [84] K. K. Wong, C. B. Chae, and K. F. Tong, “Compact ultra massive antenna array: A simple open-loop massive connectivity scheme,” *IEEE Trans. Wireless Commun.*, vol. 23, no. 6, pp. 6279–6294, Jun. 2024.
- [85] K.-K. Wong, “Transmitter CSI-free RIS-randomized CUMA for extreme massive connectivity,” *IEEE Open J. Commun. Soc.*, vol. 5, pp. 6890–6902, 2024.
- [86] N. Waqar *et al.*, “Opportunistic fluid antenna multiple access via team-inspired reinforcement learning,” *IEEE Trans. Wireless Commun.*, vol. 23, no. 9, pp. 12068–12083, Sept. 2024.

- [87] H. Hong, K. K. Wong, K. F. Tong, H. Shin, and Y. Zhang, "Coded fluid antenna multiple access over fast fading channels," *IEEE Wireless Commun. Lett.*, vol. 14, no. 4, pp. 1249–1253, Apr. 2025.
- [88] H. Hong, K. K. Wong, H. Xu, *et al.*, "Downlink OFDM-FAMA in 5G-NR systems," *IEEE Trans. Wireless Commun.*, [arxiv:2501.06974](https://arxiv.org/abs/2501.06974), 2025.
- [89] F. Rostami Ghadi *et al.*, "Fluid antenna-assisted dirty multiple access channels over composite fading," *IEEE Commun. Lett.*, vol. 28, no. 2, pp. 382–386, Feb. 2024.
- [90] J. Zou *et al.*, "Shifting the ISAC trade-off with fluid antenna systems," *IEEE Wireless Commun. Lett.*, vol. 13, no. 12, pp. 3479–3483, Dec. 2024.
- [91] C. Wang *et al.*, "Fluid antenna system liberating multiuser MIMO for ISAC via deep reinforcement learning," *IEEE Trans. Wireless Commun.*, vol. 23, no. 9, pp. 10879–10894, Sept. 2024.
- [92] F. Rostami Ghadi *et al.*, "Performance analysis of FAS-aided NOMA-ISAC: A backscattering scenario," *arXiv preprint*, [arXiv:2408.04724](https://arxiv.org/abs/2408.04724), 2024.
- [93] F. Rostami Ghadi, K.-K. Wong, K.-F. Tong and Y. Zhang, "Cache-enabled fluid antenna systems: Modeling and performance," *IEEE Commun. Lett.*, vol. 28, no. 8, pp. 1934–1938, Aug. 2024.
- [94] E. Bastug, M. Bennis, and M. Debbah, "Living on the edge: The role of proactive caching in 5G wireless networks," *IEEE Commun. Mag.*, vol. 52, no. 8, pp. 82–89, Aug. 2014.
- [95] C. Wang *et al.*, "AI-empowered fluid antenna systems: Opportunities, challenges and future directions," *IEEE Wireless Commun.*, vol. 31, no. 5, pp. 34–41, Oct. 2024.
- [96] J. Zou, S. Sun, and C. Wang, "Online learning-induced port selection for fluid antenna in dynamic channel environment," *IEEE Wireless Commun. Lett.*, vol. 13, no. 2, pp. 313–317, Feb. 2024.
- [97] W. C. Jakes and D. C. Cox, *Microwave mobile communications*. Wiley-IEEE press, 1994.
- [98] K.-K. Wong, K.-F. Tong, Y. Chen, and Y. Zhang, "Closed-form expressions for spatial correlation parameters for performance analysis of fluid antenna systems," *Elect. Lett.*, vol. 58, no. 11, pp. 454–457, Apr. 2022.
- [99] Z. Chai *et al.*, "Performance of machine learning aided fluid antenna system with improved spatial correlation model," in *Proc. IEEE 1st Int. Conf. 6G Networking (6GNet)*, pp. 1–6, Paris, France, July 2022.
- [100] M. Khammassi, A. Kammoun, and M.-S. Alouini, "A new analytical approximation of the fluid antenna system channel," *IEEE Trans. Wireless Commun.*, vol. 22, no. 12, pp. 8843–8858, Dec. 2023.
- [101] H. Xu, K.-K. Wong, W. K. New, and K.-F. Tong, "On outage probability for two-user fluid antenna multiple access," *Proc. IEEE Int. Conf. Commun. (ICC)*, pp. 2246–2251, Rome, Italy, Jun. 2023.
- [102] M. R. Akdeniz *et al.*, "Millimeter wave channel modeling and cellular capacity evaluation," *IEEE J. Sel. Areas Commun.*, vol. 32, no. 6, pp. 1164–1179, Jun. 2014.
- [103] C. Skouroumounis and I. Krikidis, "Fluid antenna with linear MMSE channel estimation for large-scale cellular networks," *IEEE Trans. Commun.*, vol. 71, no. 2, pp. 1112–1125, Feb. 2022.
- [104] C. Skouroumounis and I. Krikidis, "Large-scale fluid antenna systems with linear MMSE channel estimation" in *Proc. IEEE Int. Conf. Commun. (ICC)*, pp. 1330–1335, Seoul, Korea, Republic of, Aug. 2022.
- [105] S. Ji, C. Psomas, and J. Thompson, "Correlation-based machine learning techniques for channel estimation with fluid antennas," in *Proc. IEEE Int. Conf. Acoustics, Speech Sig. Process. (ICASSP)*, Seoul, Korea, Republic of, Apr. 2024, pp. 8891–8895.
- [106] H. Zhang *et al.*, "Learning-induced channel extrapolation for fluid antenna systems using asymmetric graph masked autoencoder," *IEEE Wireless Commun. Lett.*, vol. 13, no. 6, pp. 1665–1669, Jun. 2024.
- [107] R. Wang *et al.*, "Estimation of channel parameters for port selection in millimeter-wave fluid antenna systems," in *Proc. IEEE ICC Workshops*, Dalian, China, Aug. 2023, pp. 1–6.
- [108] W. Ma, L. Zhu, and R. Zhang, "Compressed sensing based channel estimation for movable antenna communications," *IEEE Commun. Lett.*, vol. 27, no. 10, pp. 2747–2751, Oct. 2023.
- [109] Z. Xiao *et al.*, "Channel estimation for movable antenna communication systems: A framework based on compressed sensing," *IEEE Trans. Wireless Commun.*, vol. 23, no. 9, pp. 11814–11830, Sept. 2024.
- [110] Z. Zhang, J. Zhu, L. Dai, and R. W. Heath Jr, "Successive bayesian reconstructor for channel estimation in fluid antenna systems," *IEEE Trans. Wireless Commun.*, vol. 24, no. 3, pp. 1992–2006, Mar. 2025.
- [111] Z. Guo, X. Wang, and W. Heng, "Millimeter-wave channel estimation based on 2-D beamspace MUSIC method," *IEEE trans. wireless commun.*, vol. 16, no. 8, pp. 5384–5394, Aug. 2017.
- [112] R. Roy and T. Kailath, "ESPRIT-estimation of signal parameters via rotational invariance techniques," *IEEE Trans. Acoust., Speech, Sig. Process.*, vol. 37, no. 7, pp. 984–995, Jul. 1989.
- [113] M. Haardt and J. A. Nossek, "Unitary ESPRIT: How to obtain increased estimation accuracy with a reduced computational burden," *IEEE Trans. Sig. Proc.*, vol. 43, no. 5, pp. 1232–1242, May 1995.
- [114] B. Fleury, D. Dahlhaus, R. Heddergott, and M. Tschudin, "Wideband angle of arrival estimation using the SAGE algorithm," in *Proc. IEEE ISSSTA'95*, vol. 1, Mainz, Germany, Sep. 1996, pp. 79–85.
- [115] H. Hong *et al.*, "Fluid antenna system empowering 5G NR," *arXiv preprint*, [arXiv:2503.05384](https://arxiv.org/abs/2503.05384), 2025.
- [116] G. Ozcan and M. C. Gursoy, "Optimal power control for fading channels with arbitrary input distributions and delay-sensitive traffic," *IEEE Trans. Commun.*, vol. 66, no. 9, pp. 4333–4344, Sept. 2018.
- [117] Y. Chen and I. Darwazeh, "An accurate approximation of delay with Nakagami- m channels and exponential arrivals," in *Proc. IEEE Global Commun. Conf. (GLOBECOM)*, pp. 1–6, Dec. 2015, San Diego, CA, USA.
- [118] 3GPP, "LTE; evolved universal terrestrial radio access (E-UTRA); radio frequency (RF) system scenarios," *3GPP TR 36.942 version 17.0.0 Release 17*, vol. 3, p. 107, 2022.
- [119] M. Zorzi and R. R. Rao, "Energy-constrained error control for wireless channels," *IEEE Pers. Commun.*, vol. 4, no. 6, pp. 27–33, Dec. 1997.
- [120] M. Series, "IMT vision—framework and overall objectives of the future development of IMT for 2020 and beyond," *Recommendation ITU*, vol. 2083, no. 0, 2015.
- [121] Y. Zhu, G. Zheng, L. Wang, K.-K. Wong, and L. Zhao, "Content placement in cache-enabled sub-6 GHz and millimeter-wave multi-antenna dense small cell networks," *IEEE Trans. Wireless Commun.*, vol. 17, no. 5, pp. 2843–2856, May 2018.
- [122] F. Rostami Ghadi *et al.*, "A Gaussian copula approach to the performance analysis of fluid antenna systems," *IEEE Trans. Wireless Commun.*, vol. 23, no. 11, pp. 17573–17585, Nov. 2024.